Numerical Investigations into the Seismic Behavior of Free from Damage Joints

Candidate name: Joshua Krehnbrink

Supervisors: Prof. Ph.D. Raffaele Landolfo, Assist. Prof. Ph.D. Mario D'Aniello

Co-Supervisor: Eng. Mariana Zimbru

Thesis submitted in partial fulfilment of the requirements For the Degree of Master of Science in Construction of Steel and Composite Structures European Erasmus Mundus Masters Course **Sustainable Construction Under Natural Hazards and Catastrophic Events**

University of Naples " Federico II"
Date: 1st February 2018

Numerical Investigations into the Seismic Behavior of Free from Damage Joints

Author: Joshua Krehnbrink

Supervisor: Prof. Ph.D. Raffaele Landolfo, Assist. Prof. Ph.D. Mario D'Aniello
Co-Supervisor: Eng. Mariana Zimbru

University of Naples Federico II

European Erasmus Mundus Master Course
Sustainable Constructions
Under Natural Hazards and Catastrophic Events
520121-1-2011-1-CZ-ERA MUNDUS-EMMC

STATEMENT OF THESIS APPROVAL

This thesis prepared by **Joshua Krehnbrink** entitled 'Numerical Investigation into the Seismic Behavior of Free from Damage Joints' is approved in partial fulfillment of the requirements for the degree of Master of Science by the following faculty members served as the supervisory committee chair and members.

_____, Chair _____
Date Approved

_____, Member _____
Date Approved

_____, Member _____
Date Approved

Student's signature _____

Date of Submission _____

ABSTRACT

The current strategy implemented in EN 1998 for designing buildings with resistance against seismic actions is based on capacity design principles. This method allows the formation of plastic hinges into predefined parts of the structure in the ultimate limit state, meaning there will be significant damage in critical elements of the structure. These current EC8 methods are cheap in construction, but cost a lot for rehabilitation after a seismic event. There is a need for new design strategies which improve the seismic response of structures while decreasing potential damage caused by a rare seismic event.

In the last few decades, new design methodologies have been proposed for this purpose. Efficient systems for improving seismic resistance of a structure and for minimizing damage include: shear metal panels, BRBs, viscous dampers, replaceable shear links in EBFs, and friction dissipative joints.

The last possibility of dissipative joints in structures is effective, efficient, and economical. Joints fitted with friction damping devices are not significantly larger or more costly than current seismic resisting joints. There will be no architectural interference from the friction damping device, and the cost of rehabilitating a structure fitted with such joints will be considerably reduced. This is due to the fact that FREEDAM joints dissipate energy through friction between plates in contact rather than through plastic deformation.

The aim of the FREEDAM project is to develop seismically prequalified novel types of joints which dissipate seismic energy through friction. During both numerical and empirical tests, the cyclic behavior of these joints has proven to be stable with low degradation of strength and high rotational capacity.

In this paper, the seismic behavior of FREEDAM joints is investigated using FEM methods to compare the response of a full frame fitted with FD joitns versus modern RBS joints, as well as to theoretically analyze several sub-configurations and assemblies within the FD2 joint configuration. The accuracy of assumptions made in the finite element models are also validated.

TABLE OF CONTENTS

ACKNOWLEDGEMENTS

A thesis is not the work of one person, but rather the collective efforts of a group of people. With this in mind, there are many people I would like to thank for their assistance towards the completion of this paper.

First up is Eng. Mariana Zimbru, without her help and guidance this thesis would not have been possible. Her engineering knowledge and quick wit were always available – to talk with as a colleague, but also as a friend. Thank you also to Assist. Professor Mario D'Aniello for welcoming me so warmly to Italy. It was a great pleasure to work alongside you as part of the FREEDAM team, and also to learn from you about Italian culture. I would also like to thank Eng. Roberto Tartaglia for all of his life lessons.

Thank you again Assist. Professor Mario D'Aniello, Professor Federico Mazzolani, and Professor Raffaele Landolfo, it has been such a great experience to work as part of the FREEDAM research program and to cooperate with you all.

So much respect and gratitude goes to all of the professors who made SUSCOS possible. Thank you to Professor František Wald, Professor Raffaele Landolfo, Professor Dan Dubina, Professor Luís Simões da Silva, and Professor Jean-Pierre Jaspart for being the coordinators of this program at your home universities. Also, to every single professor who spent time during lectures with us – it has been an honor and a great privilege to have learned from such top scholars. And to the administrators, especially Isabelle Noirot, for smoothing out the path for us.

A big thanks to the European Commission for supporting such a wonderful Erasmus Mundus program. The opportunities you have granted all of us have helped us succeed academically, and taught us so many life lessons we will never forget.

To my family; even though you all were not so happy that I would move away, I have always felt your support and love across all this distance. You guys have been my solid foundation through life, and will continue to be no matter where we are. Also to my friends, the ones I've met in Europe throughout my Erasmus Mundus experience and the ones back home in the US. You guys have been the one thing keeping me sane through SUSCOS!

A very special thanks goes out to all my SUSCOS family. Over the past year and a half, we've spent countless days in the classroom together, too many late nights studying, and most importantly we were always there for each other. It's something significant when so many people can come together from different countries and cultures, and learn to care about each other like family. I will forever cherish all of the memories we've made together, and wish everyone good luck in the future. See you in Prague!

Chapter I: INTRODUCTION

1.1 Motivation

As the research for this paper is conducted within the framework of the FREEDAM European Research Project, the motivation and objectives remain the same.

Current buildings in Europe are designed according to Eurocode EN1998 (approved 2004), which deals with designing structures for resistance to earthquakes. The fundamental requirements put forward in these codes deal with limit state design, wherein the structure must be designed to withstand a certain amount of structural damage.

Joints have a large impact on the overall seismic performance/failure of a structure. In the current accepted practice of capacity design, the engineer is responsible for determining which critical elements within a structure will plastically deform during a strong seismic event. While this method will maintain the proper performance level as intended by the designer, it can lead to significant structural damage.

Traditionally, dissipate seismic energy through plastic deformation of either:

1. Partial Strength Connections, which allow for plasticization of some components, or
2. Beams, which are designed to develop plastic hinges near the joint.

The capacity design method concedes large amounts of damage in important structural members for rare seismic events. This translates to either a large rehabilitation cost to get the building operational again, or the possibility that the building has to be demolished if it is deemed uneconomical to rehab.

Contrary to these traditional design methods, structures (MRFs) equipped with FREE from DAMage (FREEDAM) joints use partial strength joints with energy dissipation through friction. The FREEDAM joints have similar characteristics to typical beam-column partial-strength connections in terms of moment resistance and rotation capacity, meaning they will not have a detrimental effect on the total capacity of the building. It is possible, however, by adjusting the number of bolts and clamping force in the dissipative connection, to keep major damage out of the critical elements of the joint (beam, column, haunch, etc.). Instead, some plastic damage will occur at the web-flange interface in the T-stubs or top flange plates, with other minor elements such as bolts experiencing inelastic deformations. Plastic deformation in these joints is constrained to the replaceable elements, specifically the bolts and shims of the friction damping device. Current codes need to be revised to allow for a change of the dissipation mechanism from plastic hinges to sliding.

1.2 Objectives

When testing new joint typologies, it is imperative to not only run accurate tests and simulations, but to also do this in a time- and cost-efficient manner. Therefore, as part of the FREEDAM Project funded by the European commission, the scope of this thesis follows the same objectives. The overall goal is to achieve a better understanding of the behavior of FREEDAM joints, and to numerically analyze the behaviors of different joint assemblies. This can be realized through the following objectives of this paper:

- to understand the difference between frames equipped with RBS MRF joints compared to frames equipped with FREEDAM joints
- to model and determine the response of FD-2 joints when modeled with different assembly and joint geometries
- to explore and determine the effects of different parameters on the response of FD joints.

Through numerical analysis using FEM software, it is possible to advance these objectives towards the final goal of the FREEDAM project.

1.3 Steps of research

Throughout the phases of this thesis, different investigations were performed as the research proceeded and new ideas or variables were experimented with. The steps towards realizing the objectives were performed in the following order:

First, as one of the main purposes of the project is to investigate the response of FREEDAM joints in comparison to standard RBS joints, it is critical to have a model of sufficient scale and accuracy to properly compare the responses. As a multi-story frame was desired for this comparison, it became necessary to find a way to reduce the number of finite elements in the model. The solution was to investigate the use of wire elements for modeling sections of the beam and column.

Next, the full scale RBS and FD MRF frames were modeled in one and two stories. However, before performing the analyses, it was imperative to ensure the FE models came as close as possible to representing the real behavior of the frames. In order to guarantee this, certain variables within the models were calibrated according to previously obtained empirical results.

During this process of calibration, another question arose: would the addition of washerplates to the FD device deliver a more uniform clamping force, and thus positively affect the seismic behavior of the joint? This addition of using washerplates in the friction damping device was investigated.

After the calibration phase, finally the one and two story RBS MRF frames were compared against similar frames fitted with FD joints, and their responses recorded. Along with this comparison, a numerical analysis of six FD2 joint assemblies was performed.

Chapter II: STATE OF THE ART

Earthquakes are some of the most extreme natural disasters to occur in modern times. They can level cities, destroy cultural sites, cause huge economic losses, and most significantly are capable of causing a huge loss of life. The **United States Geological Survey** estimates that there are over two hundred magnitude 6+ earthquakes every year, which cause significant damage and potentially collapsing even well-built structures. It is only with the instruments and technologies of the last century that we are able to accurately measure, classify, and implement safety mechanisms to drastically reduce the damage caused by rare seismic events.

Magnitude	**Description**	**Average earthquake effects**	**Average frequency of occurrence (estimated)**
1.0–1.9	Micro	Micro earthquakes, not felt, or felt rarely. Recorded by seismographs.[16]	Continual/several million per year
2.0–2.9	Minor	Felt slightly by some people. No damage to buildings.	Over one million per year
3.0–3.9		Often felt by people, but very rarely causes damage.	Over 100,000 per year
4.0–4.9	Light	Noticeable shaking of indoor objects and rattling noises. Generally causes none to minimal damage.	10,000 to 15,000 per year
5.0–5.9	Moderate	Can cause damage of varying severity to poorly constructed buildings.	1,000 to 1,500 per year
6.0–6.9	Strong	Damage to a moderate number of well-built structures in populated areas. Earthquake-resistant structures survive with slight to moderate damage.	100 to 200 per year
7.0–7.9	Major	Causes damage to most buildings, some to partially or completely collapse or receive severe damage. Well-designed structures are likely to receive damage.	10 to 20 per year
8.0–8.9	Great	Major damage to buildings, structures likely to be destroyed. Will cause moderate to heavy damage to sturdy or earthquake-resistant buildings.	One per year
9.0 and greater		At or near total destruction – severe damage or collapse to all buildings. Heavy damage and shaking extends to distant locations. Permanent changes in ground topography.	One per 10 to 50 years

Table II.1: Earthquake descriptions and frequencies by magnitude, (United States Geological Survey)

Some of the most recent technological advances come in the form of computing capacity and software which allows us to accurately analyze a structure. General advancements in the field of Finite Element Modeling (FEM) have made the process even more accurate, so that numerical models match the empirical results, possibly with small adjustments. FEM not only allows the results to be predicted to a certain degree of accuracy, but it can also be used gauge as to determine whether or not the outputs from the experimental tests can be considered as valid.

With the use of finite element analyses and numerical modeling, we are able to efficiently test and compare new methods to minimize the seismic response of modern buildings.

Relatively new systems for improving seismic resistance of a structure and for minimizing damage include using shear metal panels, BRBs, viscous dampers, replaceable shear links in EBFs, and friction dissipative joints.

The following papers represent past works completed towards the investigation, the behavior, and the modifications to friction dissipative joints in structures.

Starting in the last few decades, a new focus in seismic resisting systems has been the push towards designing and developing a new type of moment resistant joint which utilizes friction as the main method of energy dissipation. The first modern structural joint designed to dissipate seismic energy through friction was developed by **Clifton C., 2005**. In the Sliding Hinge Joint (SHJ), the beam is pinned to the column through the top flange plate (or T-stub), which acts as the point of rotation. It was developed by Clifton as a low-damage alternative to traditional welded connections. An important theory behind these joints is that they decouple strength from stiffness. Traditionally, a stronger joint meant also a stiffer one; however with friction based dissipative connections, the joint is allowed a large rotation and inelastic deformations in the minor components, while maintaining a large portion of its capacity. This is achieved through sliding in the friction components, which greatly reduces the inelastic demand in the beam and the column.

Due to necessary slip force needed to overcome static friction, the SHJ is actually designed to remain static under service level earthquakes (Service Limit State). The joint will only engage in dynamic action under design level earthquakes (Ultimate Limit State). Additionally, under maximum earthquake events, the bolts may hit the end of the slotted holes, thus engaging in plastic deformation and adding significant capacity to the joint; however a major loss in bolt pretension occurs.

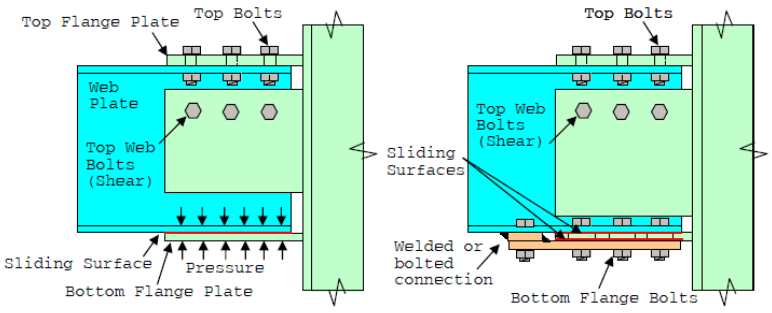

Figure II.1: Typical geometry of SHJs, (Clifton, MacRae and Mackinven)

Clifton et al., 2007, describes the beam-column SHJ as having an asymmetric double sliding surface with a large rotational capacity and almost no damage. Here, rotation occurs about the fixed top flange, while sliding occurs directly on the bottom flange of the beam. Clifton et al. put forth several joint typologies, all considering the same principles.

These types of joints produce a non-rectangular hysteric loop. This is due to the fact that first one friction surface is engaged until the friction capacity is reached, and then the second friction surface is engaged. This behavior creates a step-like hysteric loop, which implies lower permanent deformation of the structure after a seismic event.
This joint can be considered a predecessor to the FREEDAM joints analyzed in this paper. While there are some differences, it contains the same rotation mechanism in the top flange plate and sliding mechanism on the bottom of the connection.

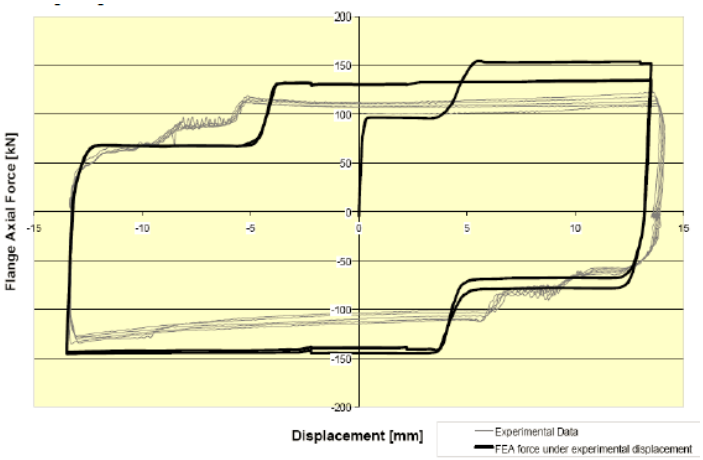

Figure II.2: Hysteric behavior of SHJ, (Clifton, MacRae and Mack

While it is beneficial for the structure to have dissipative connections at the beam-column connections, the most critical points in the structure are at the column bases. If the joints and braces are dissipative, but the column base undergoes inelastic deformations during a seismic event, the whole structure could need to be replaced anyways.

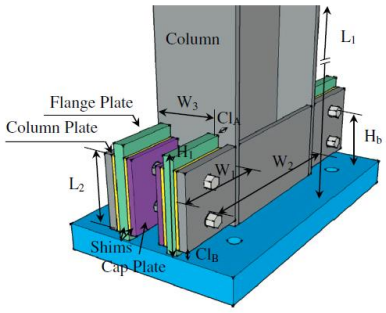

Figure II.3: WAFC geometry, (J. Borzouie, G. MacRae and G. Rodgers)

With this in mind, **Borzouie et al., 2015**, performed empirical tests on the performance of a column base with a weak axis aligned asymmetric friction connection (WAFC). In the WAFC connection, the column and base plate are in full contact, but without direct welding. Instead, plates are welded to the column flange parallel to the weak axis of the column, and these plates are bolted with slotted holes to another set of plates welded to the base plate. When a cyclical force is applied along the connection's strong axis, the resulting hysteric loop was shown to have a step-shaped response. The step shape is characteristic from having two independently activated slip surfaces per plate, similar to the first iterations of the SHJ.

The testing concluded that the base connection did not have significant strength degradation even after 4% of drift. There was no substantial damage to the column or baseplate, meaning the connection can be classified as low damage. Another significant benefit to having friction dissipative device in the column base is having the option to untighten the bolts of the AFC to allow for the removal of post-earthquake residual displacement.

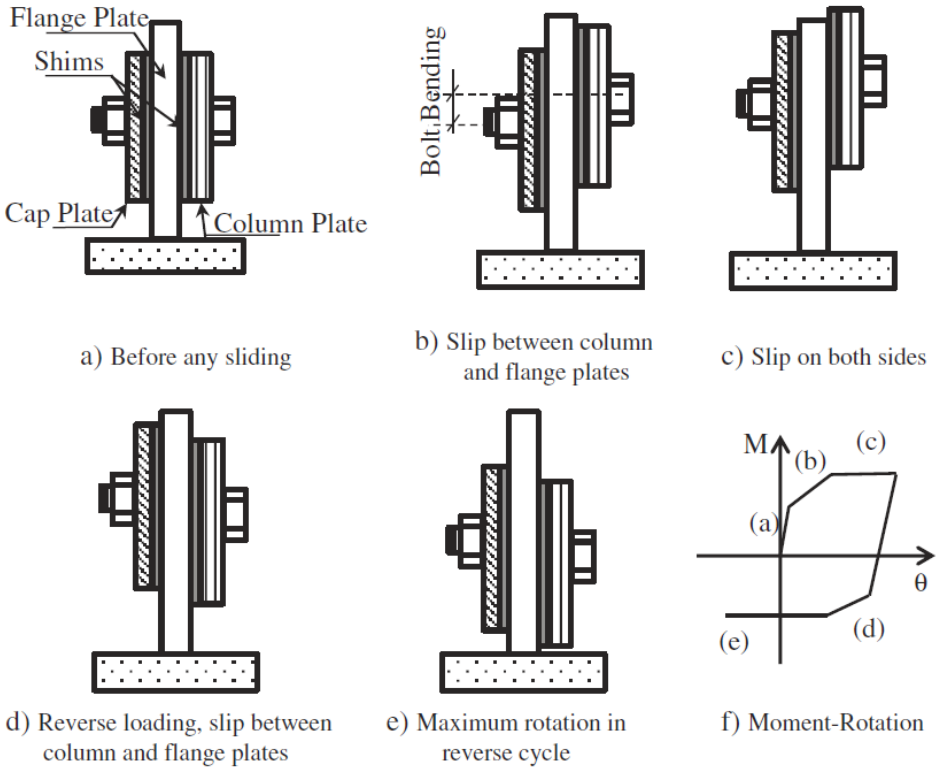

Figure II.4: Behavior of SHJ with two slip surfaces, (J. Borzouie, G. MacRae and G. Rodger

Similar to the WAFC, **Borzouie et al., 2016** also performed experiments verifying the behavior of a column base fitted with a Strong-axis Asymmetric Friction Connection (SAFC). Similar to the previous study, the column is in direct contact with the base plate, but is not immediately

connected to it. In these column base connections, the three mechanisms which provide moment resistance in this frame are: axial force, prying, and sliding of the column.

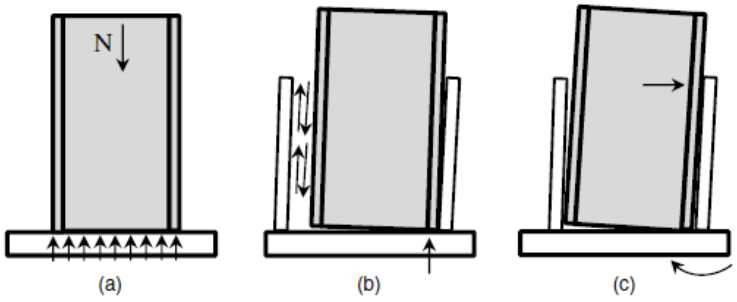

Figure II.5: Mechanisms of load transfer at the column base: (a) axial force, (b) sliding, (c) prying, (J. Borzouie, G. MacRae and J. Chase)

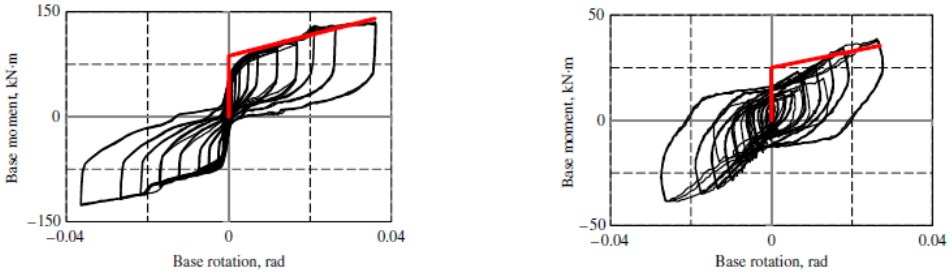

Figure II.6: Moment rotation diagram of the base about: LEFT - strong axis under axial force; RIGHT - weak axis under axial force, (J. Borzouie, G. MacRae and J. Chase)

As shown in Figure II.6, several cycles of up to 0.04 rad were performed without capacity loss in the connection. Along with these results, cycles with axial force in a clover-leaf pattern resulted in deformation of the flange tips, which reduce the initial stiffness.

While the effectiveness of the SHJ has been accepted, it was unclear about the behavior of the joint under multiple seismic events. The flange plates especially are critical, as subjecting the plates and welds to inelastic deformation could compromise their capacity during future events. Therefore, **Khoo et al., 2013** analyzed these plates with low cycle, high rotation fatigue tests to determine their remaining strength. Along with this, it should be kept in mind that the plates are sized to suppress the failure components listed in the Component Method in EN 1993.

The testing was conducted using only low cycle fatigue, with no focus on high cyclic seismic events. However, the analysis concluded that the plates can conservatively undergo at least six design level seismic events before needing to be replaced, and is thus acceptable. This number surely exceeds the expected building life.

Even though low-damage or free-from-damage joints can ensure the main structural components undergo only elastic deformation, they don't necessarily ensure that the structure will be brought back to center. For this purpose, **Khoo et al., 2012** explored using friction ring springs in order to counter this problem through the creation of the Self-Centered Sliding Hinge Joint (SCSHJ). Ring springs can be preloaded, and dissipate 2/3 of their energy through friction sliding of the rings, with about 1/3 of the energy being stored as compression/tension. In theory, the ring springs can be used for three useful purposes: 1) by dissipating some of the energy through friction, it increases the moment capacity of the joint; 2) energy stored in the spring can aid in self-centering after a seismic event; and 3) elastic strength of the joint can be preserved after pretension loss in the clamping bolts, due to the pretension in the springs.

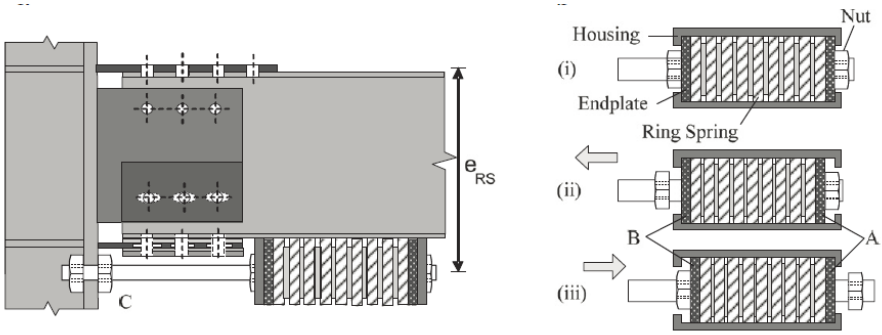

Figure II.7: SCSHJ layout and spring ring assembly, (H.-H. Khoo, C. Clifton and J. Butterworth)

After using 2D nonlinear analysis to compare five different frames, they discovered that with the use of ring springs in the SCSHJ, residual drifts in the studied structures were limited to 0.1% when the ring spring was designed to carry 40% of the total moment capacity.

Under cyclic loading, the SCSHJ behavior can be seen as a combination of the standard SHJ and flag-shaped ring spring behaviors. Increasing the percentage of bending moment capacity carried by the spring generally had little effect on peak displacement, but it significantly reduced the residual displacements as a result of increasing pinching of the hysteresis loop.

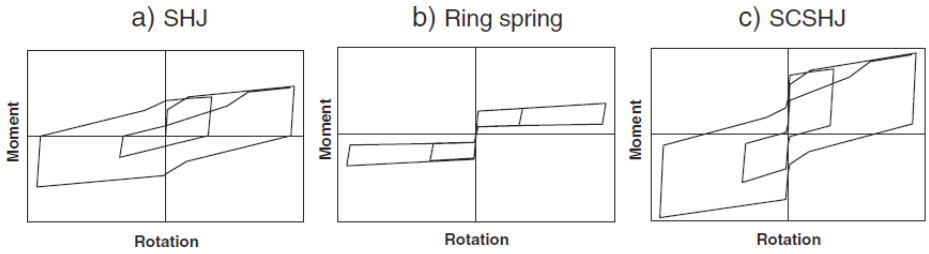

Figure II.8: Idealised moment rotational behavior, (H.-H. Khoo, C. Clifton and J. Butterworth)

As mentioned before, with the use of these springs the residual drift can be limited to 0.1%, which is within the stated construction tolerance in the Eurocodes of 0.2%. While this research documented how ring springs can be used to increase the moment capacity of a connection and

aid in recentering a building, the economical aspect was not considered. A real cost analysis needs to be undertaken to determine if this is a practical solution for dissipative joints.

During seismic events, all of the inelastic deformation occurs in the beam-column flange cleats, as well as in the bolts. A critical aspect of any friction connection then is to consider whether the bolts experience pretension loss and inelastic deformation. **Khoo et al., (2014)** studied the additional plasticity induced in these pretensioned bolts due to the applied moment-shear-axial force interaction to determine how much dissipative capacity was lost during a seismic event. Figure II.9 shows the idealized external forces on the pretensioned bolt.

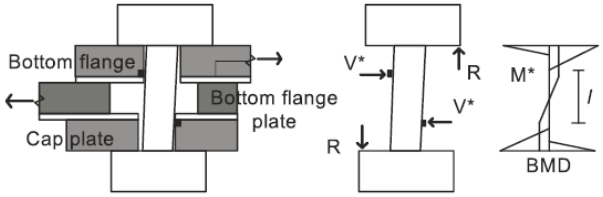

Figure II.9: AFC idealized bolt deformation, external forces, and bending moment distribution, (H.-h. Khoo, C. Clifton and G. MacRae)

The study performed experimental tests and created multiple methods to model this interaction, and in the end both proved to be accurate to determine bolt capacity. Based on the test results, it was then determined that a strength reduction factor of $\phi_{AFC} = 0.75$ and an overstrength factor of $\phi o_{,AFC} = 1.4$ is reasonable in the design of the AFC.

The work of the previous authors helped to set the precedent for the FREEDAM project funded by the European Commission. FREEDAM joints are beam-column connections which cover two configuration types and range over multiple assembly sizes. The unique element in these joints is a device located below the beam, which dissipates seismic energy through friction. The friction damper remains static during a small seismic event, and becomes dynamic during a design level earthquake. In order to determine the friction resistance necessary for such joints, the Coulomb friction equation was applied to determine the necessary parameters:

$$F_{slip} = \mu \cdot \eta_s \cdot \eta_b \cdot N_b$$

Where μ is the dynamic friction coefficient, η_s is the number of slip surfaces, η_b is the number of bolts, and N_b is the pretension force applied to the bolts. The most influential variable in this formula is the friction coefficient, which depends on the surface treatment of the slip surface as well as the material properties. The pretension force in the bolts, N_b, is the most sensitive variable in the equation. It has been proven that the joint capacity depends linearly on the pretensioned force applied in the bolts, however the pretensioning method is not precise and there will be some variation. Along with this, there is the worry about long term relaxation which could significantly reduce the dissipative capacity of the joints; this is one area that should

be explored in future research. Nonetheless, empirical tests have accurately predicted the response of friction dissipative connections.

Once the design moment resistance is calculated, we are able to determine the desired slip force. Once this and dynamic friction coefficient are known, it is possible to modify the other variables in order to design the required friction damping device. However, because FD-MRF joints dissipate seismic energy through a different mechanism than standard MRF joints, a new design methodology must be proposed. **Zimbru et al., 2017** examines two methods for determining the F_{slip} required from the FREEDAM joint. Similar to capacity design, these methods of calculation must ensure that the capacity of the friction damping device is less than the beam or column, in order to realize proper joint response and to keep the critical elements elastic.

1. The first method, FD-A, for calculating the capacity of the joint assumes that the forces carried by the damper corresponds to the formation of bending strength in the beam. The slip force is a function of the design plastic bending resistance of the beam and the connection lever arm.

   $$F_{slip} = \frac{M_{pl,b,Rd}}{h_{tot}}$$

   Where $M_{pl,b,Rd}$ is the beam plastic bending resistance and h_{tot} is the connection lever arm (distance from the middle of the T-stub to the middle of the haunch bottom flange).

2. The second method, FD-B, assumes that the friction damper is designed using the forces from the seismic combination obtained from the elastic analysis.

   $$E_d = E_{d,G} + \Omega_\mu \cdot E_{d,E}$$

Where E_d is the design force for the non-dissipative element, $E_{d,G}$ is the design force coming from the gravitational loads, Ω_μ is the overstrength factor. To stay on the conservative side of calculations, it is necessary to account for difference in μ and the sensitivity of bolt pretensioning with this overstrength factor. Therefore, Ω_μ is applied to both methods:

$$\Omega_\mu = \frac{\mu_{st.95\%}}{\mu_{dyn.5\%}} * \frac{N_{b.95\%}}{N_{b.5\%}}$$

Where $\mu_{dyn.5\%}$ and $N_{b.5\%}$ are lower-bound values of dynamic friction coefficient and tightening force, and $\mu_{st.95\%}$ and $N_{b.95\%}$ are the upper-bound values.

After the development of FD-A and FD-B, both methods were compared to EC-8 using static and dynamic nonlinear analysis. The static pushover analysis showed the overall overstrength of each method.

From the static nonlinear analysis, it can be seen that FD-A method leads to frames with similar overstrength to EC8, while FD-B leads to much smaller overstrength and is more efficient. From the nonlinear dynamic analysis, it was discovered that all methods lead to a seismic demand (dealing with Transient Interstory Drift and Residual Interstory Drift) smaller than the initial sway imperfection recommended by EC3-1-1, meaning the residual displacements are negligible.

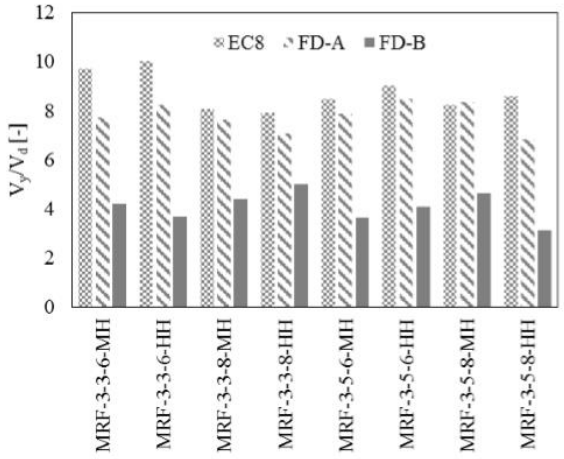

Figure II.10: Pushover results comparison for overdesign, (Zimbru, D'Aniello and Ca

From the results, it can be determined that FD-A > EC8 > FD-B in terms of material consumption. The FD-B methodology leads to frames that are more efficient with lower overdesign.

While the most economical design methodology for FD MRF's has been determined, it is critical to better understand the factors affecting the slip force for the friction device. **D'Aniello et al., 2017** sought to analyze the impact of variables from the Coulomb friction equation. Two configurations and two assemblies of FREEDAM joints using FEM methods were compared, with the joints being modeled in ABAQUS using C3D8R linear brick elements and compared using Von Mises stresses.

The main objective of this research was to investigate two parameters which have the greatest influence on friction damping devices: the dynamic friction coefficient, μ, and the bolt clamping force, N_b. Tested values of the dynamic friction coefficient include the mean value as well as values two standard deviations away from the mean, given as: $\mu_{5\%} = 0.53$, $\mu_{avg} = 0.59$, and

$\mu_{95\%} = 0.64$. Values examined for the bolt clamping force are N_b which corresponds to the design clamping force, as well as $0.5N_b$ and $1.5N_b$.

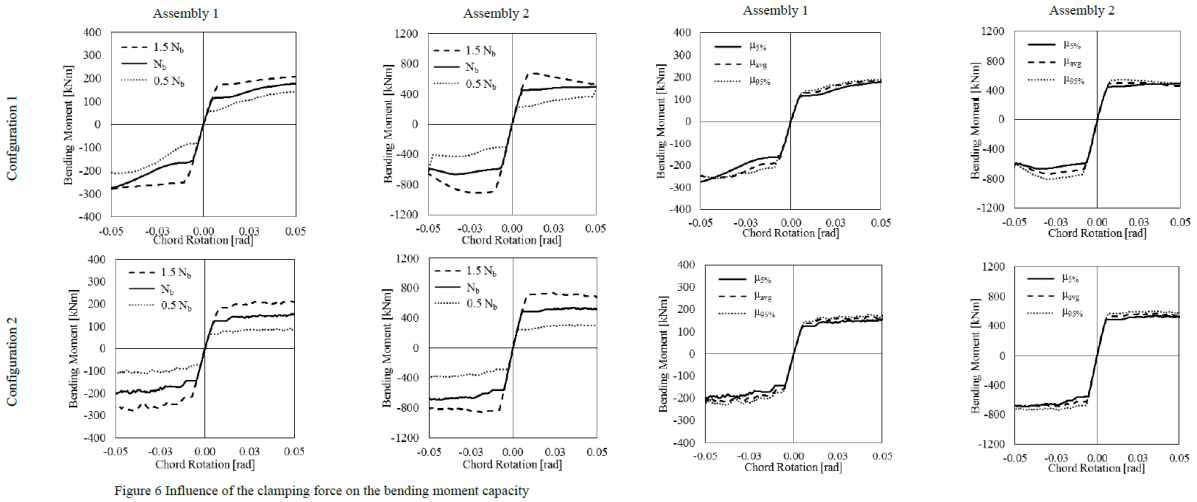

Figure II.11: LEFT 4 - Influence of clamping force on the bending moment capacity; RIGHT - Influence of dynamic frictior bending moment capacity, (D'Aniello, Mario et al.)

As can be seen from the results in Figure II.11, the clamping force massively affects the strength of the joints; bending moment capacity depends linearly on the tightening force in the bolts. $N_{b.50\%}$ corresponds to ~50% decrease in capacity while $N_{b.150\%}$ corresponds to ~50% increase in capacity. A smaller, but also significant effect is that the capacity also increases with a higher dynamic friction coefficient; however the scaling is much lower. To be conservative, the friction coefficient of 0.53 corresponding to $\mu_{5\%}$ is used for the design of FREEDAM joints. Another significant finding is that the joints with shallow beams exhibit post-yielding hardening, while joints with deeper beams exhibit post-yielding softening. The strain softening is problematic, as it leads to a significant reduction in capacity after one load cycle, especially for higher values of N_b.

While the factors affecting joint response are now known, it is important to devlope design criteria for possible new joint types. **D'Aniello et al., 2017** performed numerical analysis on the two configurations of FREEDAM joints and two assemblies for each configuration to compare the static and dynamic behavior to determine which has a more favorable response. By performing static and dynamic nonlinear analyses on the joints, they were able to compare the reactions.

Based on Figure II.13 and Figure II.12, they were able to draw the following conclusions. It is easy to notice that the response of joints are asymmetric, where there is a significant difference between the hogging and sagging bending moment capacities. However, it can also be noticed

that FD2 is more symmetric than FD1, which has a sagging moment only 14% small than hogging, compared to FD1, which reaches values 27% smaller in sagging than hogging. This difference in responses is due to the different stiffnesses of each system, and it is important as the joint is desired to be as symmetric as possible.

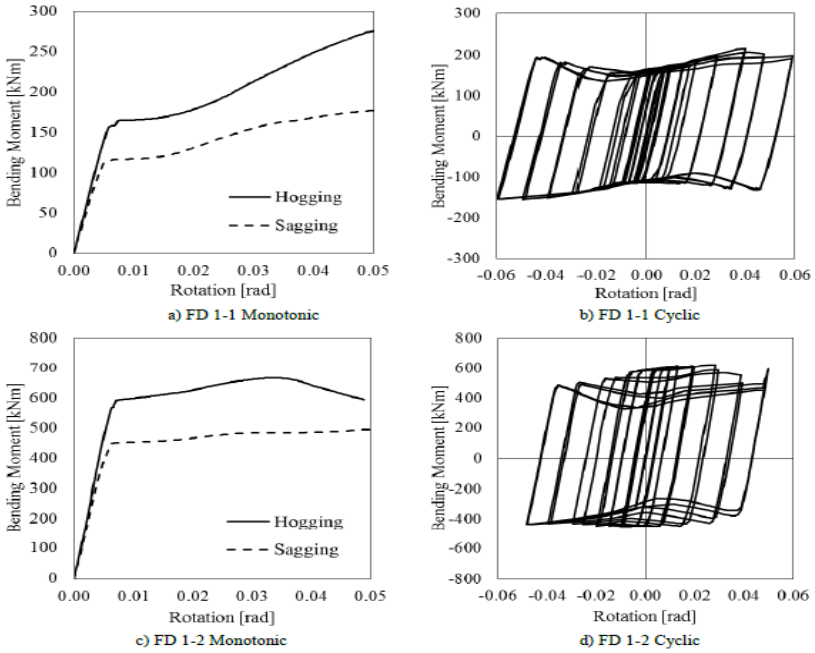

Figure II.12: Monotonic and cyclic nonlinear response of FD1-X, (D'Aniello, Zim

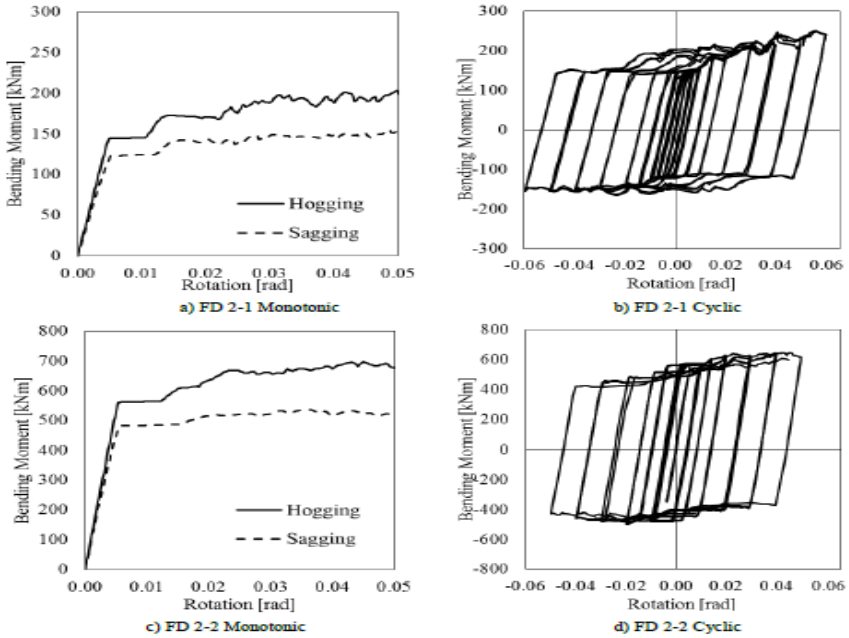

Figure II.13: Monotonic and cyclic response of FD2-X, (D'Aniello, Zimbru and La

MAIN POINTS

- FREEDAM joints are a type of AFC. AFC's are important because they have proven to have stable, repeatable, and predictable hysteric behavior.
- FD MRF joints are beneficial because they
    - decouple the moment capacity from frame stiffness, allowing more ductile joints
    - confine the inelastic seismic demands to minor joint components such as T-stub, L-stub, and bolts
    - improve the dynamic-seismic recentering ability
    - lower constructions costs
- The AFCs are designed to be rigid under serviceability level events (SLE), slide under design level earthquake (DLE) loadings, and return to an effectively rigid connection at the end of the earthquake shaking.
- Nevertheless, AFC's are subject to residual drifts and elastic strength loss following a seismic event. The drift, however, can be limited and even negated with the use of friction ring springs.
- All of the papers regarding low-damage joints have mentioned the necessity to have a dissipative joint which is similar in construction costs to a typical joint. This is a critical issue, if the joints are to be accepted and used by the design/construction community.
- While AFC's can have extremely favorable seismic responses, the slip force, F_{slip}, can be difficult to accurately determine.
    - Bolt strength is highly variable, as they are mass produced and designed to meet minimum strength requirements, with little control for their upper bounds
    - Coefficient of friction is also highly variable, as it depends on what occurs once the plates start sliding, such as ex. debris being caught between the plates and the wear patterns. Surface preparation does not significantly change this coefficient.
- While there are still overstrength and material safety factors, it is necessary to keep the moment resistance of the friction device lower than the design moment resistance of the beam.

In the future, full scale experimental tests considering frames or entire structures should be performed to compare the dynamic response of FD joints to the response of modern MRF joints, such as the RBS. A wide range of assembly sizes and geometries should be further tested to determine the response for joints that can be applicable in any size project. Finally, additions to the Eurocode should be made to account for seismic energy dissipation through sliding.

Chapter III: THE FINITE ELEMENT MODELS

The finite element analysis software used for this project is ABAQUS. The geometry of all the models was first created in AutoCAD 2013 and then the parts were imported into the FEA software. They were then modelled and analyzed using the procedure described below.

3.1 ABAQUS Procedure

Units of Measurement

ABAQUS does not consider any units; in theory, all inputs are unit-less. Therefore, it is important for the engineer to pick a unit convention in the beginning and maintain it throughout the analysis. The theoretical units that were considered during this project were as follows:

Table III.1: Units used in ABAQUS

Length	Force	Time	Stress	Mass Density	Young's Modulus
mm	*N*	*s*	*MPa (N/mm^2)*	*kg/mm^3*	*MPa (N/mm^2)*

Finite Element Type

The element type used during the FEA is the incompatible mode eight-node brick element C3D8I. This element was selected because it can effectively avoid shear locking as well as volumetric locking, as compared to the element C3D8R (Dhondt 2014). This is due to bubble functions being used in addition to the standard shape functions, which have a zero value at all nodes and nonzero values in between. Because C3D8I elements are fully integrated in this way, they are able to accurately capture the stresses due to bending.

Geometry

All of the solid elements were first drafted in AutoCAD, and later imported into ABAQUS for analysis. The wire elements were created directly in ABAQUS using a planar wire part. Each element was modeled according to their actual dimensions, with a few simplified exceptions, discussed hereafter.

Materials

Once created, the parts were assigned certain properties. Four total materials were created in ABAQUS; all materials have a mass density of 7.85e-06 kg/mm^3, congruent to the density of steel. Grade 10.9 steel was used for the bolts, and S355 for all of the elements. In models with additional web plates welded to the column, S460 was used to model weld steel. When modeling the material properties of steel, it is important to remember that while manufacturers control the

lower limit of steel to ensure it has proper capacity, there is often little to no control over the upper limits of the material strength. This fact needs to be taken into account, in order to correctly model the material and ensure the joint does not overcome the capacity of any of the structural elements. In order to achieve the most realistic analysis possible, the Elasto-Plastic response of steel was defined based on previous experimental data for the response of the different steel grades, as reported in current literature.

Table III.2: Material properties

Material	Density	Young's Modulus	f_y	ε_y	f_u	ε_u	Poisson's ratio
-	kg/mm^3	N/mm^2	N/mm^2	%	N/mm^2	%	-
S355	7.85e-6	210000	444	0.002	752	0.28	0.3
s460			460	.002	590	0.3	0.3
Grade 10.9		Variable					0.1

Steel S355

The following results were obtained through previous material testing in research carried out outside of the current project. To define the plastic range, a "Combined" (meaning isotropic + kinematic) plastic hardening model was selected in ABAQUS.

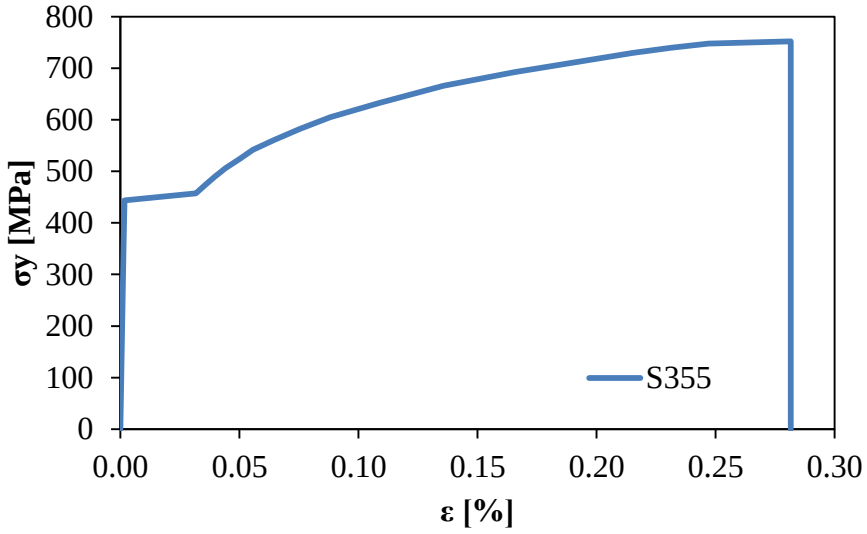

Figure III.1: S355 elasto-plastic stress-strain relation

While the nominal yield strength is 355 MPa, real practice shows the average values for the material strength are about 25% larger. In order to be as accurate as possible, the models need to take this extra capacity into account.

Steel S460

The specific material behavior for the weld steel on the Additional Web Panel is important for the accuracy of the model, however its effect on the overall behavior of the joint is insignificant. Thus, the S460 steel was simply defined as Elastic-Linearly Plastic.

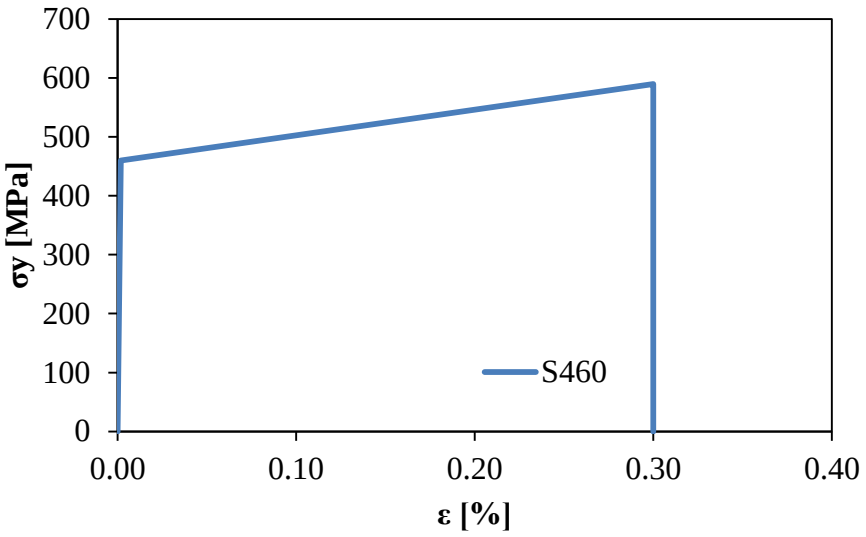

Figure III.2: S460 elasto-perfectly plastic stress strain relation

Bolt Steel, Grade 10.9

Many types of bolt classes were used in the models, ranging from M16 to M36. All classes are low carbon, high strength Grade 10.9 steel. The stress-strain curve for this material was obtained through previous material testing. Properties of Grade 10.9 steel are a proof Young's Modulus of 210000 MPa and Poisson's ratio of 0.3.

The bolt shanks, nuts, and heads were modeled in AutoCAD as perfect cylinders. For the shank specifically, the nominal gross bolt diameter was used without considering the bolt thread; therefore the bolt steel properties have to be modified in to reflect more realistic values.

As the threaded diameter of the shank is smaller than the nominal gross diameter, we must use the ratio between the effective and gross area to reduce the nominal bolt strength to mimic this difference. The material strength can be scaled as follows:

$$f_{eff} = f_{actual} \cdot \frac{A_{eff}}{A_{gross}}$$

Where:

f_{eff} is the effective stress

f_{actual} is the actual stress

A_{eff} is the area of the threaded region

A_{gross} is the gross cross sectional area

From observing the ratios in Figure III.3, we can see the ratios of effective to gross area for each bolt class. Therefore, only one stress-strain curve had to be modified with this ratio, which is shown below.

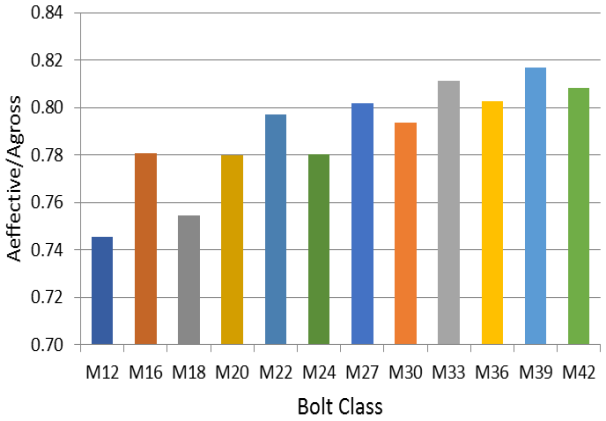

Figure III.3: Ratios between effective and gross bolt

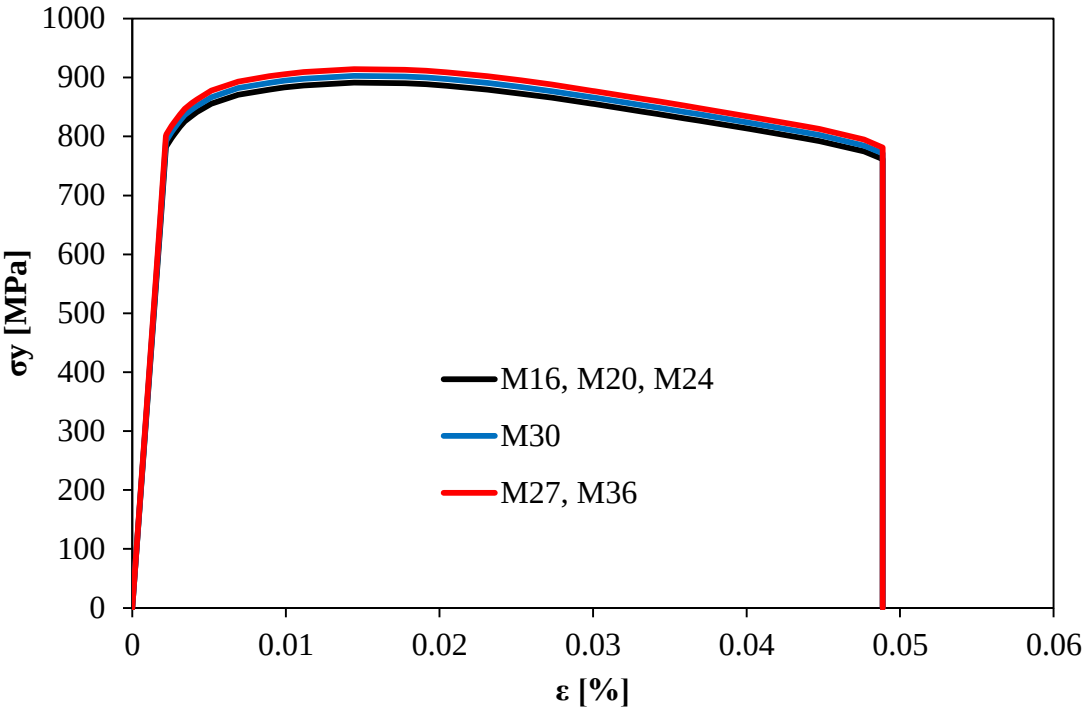

Figure III.4: Steel grade 10.9 stress-strain relation

While the strength of these simplified bolts now mimics the effective strength of a bolt with threads, the stiffness still remains unchanged. To make the stiffness of the gross area bolt shank similar to the stiffness of the net area, the equivalent elastic modulus of each bolt class must be implemented into ABAQUS. The elastic stiffness of each bolt can be calculated using the following formula from **Swanson & T. Leon (2010)**.

$$\frac{1}{K_b} = \frac{f \cdot d_b}{A_b E} + \frac{L_s}{A_b E} + \frac{L_{tg}}{A_{be} E} + \frac{f \cdot d_b}{A_{be} E} \qquad ()$$

Where:

K_b is the elastic bolt stiffness
f is the stiffness correlation factor, taken as 0.55
d_b is the nominal diameter of the bolt
A_b is the nominal cross sectional area of the bolt
E is the modulus of elasticity
L_s is the shank length of the bolt
L_{tg} is the length of the threaded portion included in the bolt's grip
A_{be} is the effective area of the threads

While the Young's Modulus should be adjusted based on the real bolt stiffness, the minimum value is 130000 MPa and it was used throughout the numerical study as a conservative assumption.

The pretensioning force applied to each bolt is also obviously corresponding to the diameter of the bolt shank. Approximately 70% of the ultimate tensile strength of the bolt is used for this application, as shown in the following equation.

$$N_b = 0.7 \cdot f_u \cdot A_s$$

Where f_u is the ultimate material strength, A_s is the area of the bolt shank, and N_b is the tensile force applied to the bolt. The bolt pretension forces can be seen in Table III.3.

Table III.3: Bolt pretension force

Bolt Class	Pretension Force [kN]
M16	110
M20	172
M24	247
M27	321
M30	393
M36	572

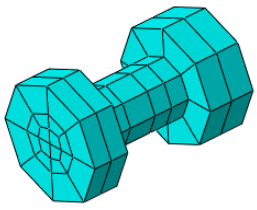

Figure III.5: Mesh of perfectly cy

Calibrating of the Web and Flange Steel

It can be expected that, due to manufacturing technology in general, the yield strength of each cross-section segment will be different. In order to be as accurate as possible, the flange and web material for IPE270 and HEB200 have been previously calibrated, and will be used in the

comparison of FD MRF to RBS MRF frames. The actual (measured) yield strength of the individual parts were larger than the nominal values, except in the case of the beam flange. The empirical testing of these materials can be seen below.

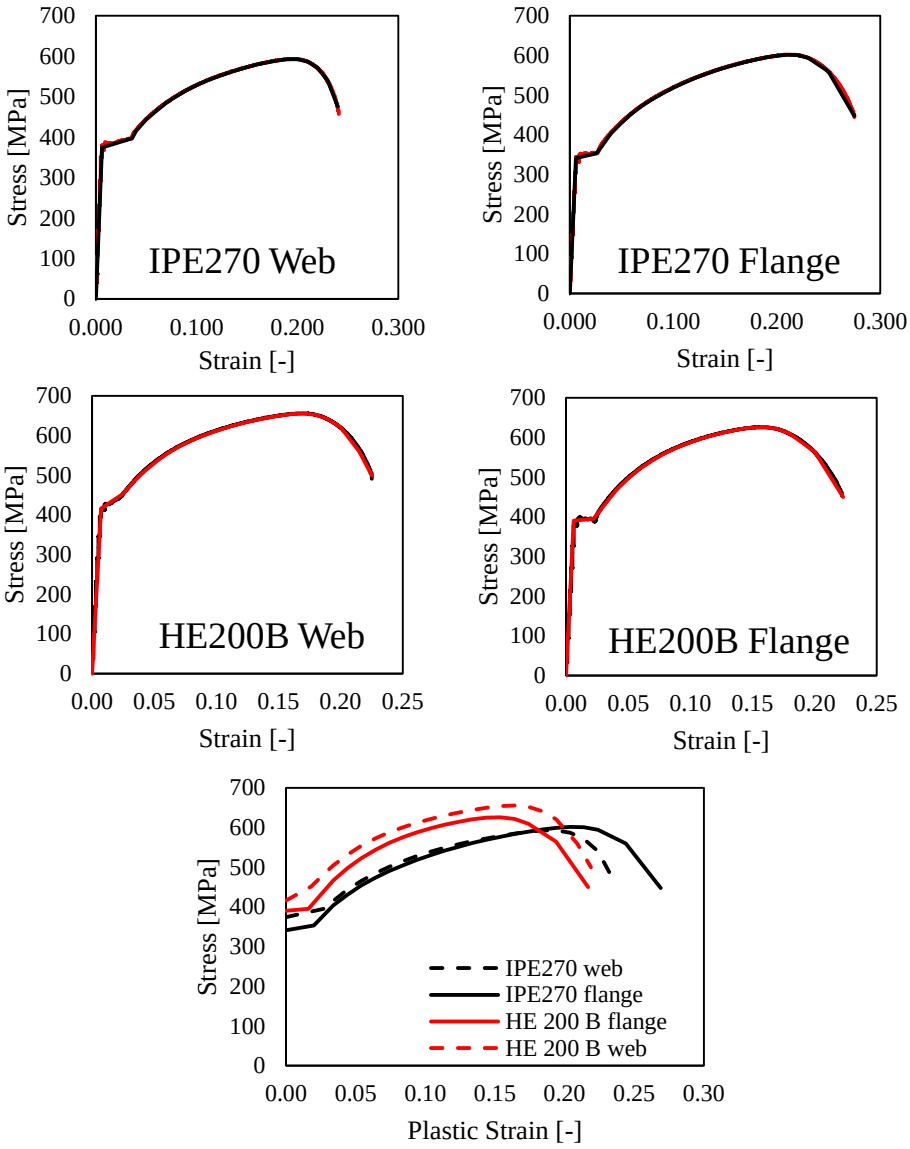

Figure III.6: Empirical sectional material properties for IPE 270 and .

For the sake of time, only these models have the cross-sectional properties modified; the other numerical analysis of six FD joint assemblies use the nominal properties of S355 for the beams and columns. In the future, a more in-depth analysis can be done on these joints using sectional steel properties derived from empirical results.

Sections

Four section types were required to define the parts in ABAQUS.

1. *S355 Steel (solid, homogenous)* was used for the solid steel elements. This section uses all the properties of S355 as well as a "combined" (isotropic + kinematic) plastic hardening model.

2. *Grade 10.9 High Strength Steel (solid, homogenous)* was used for the bolts. This section uses all the properties of S355 as well as a "combined" plastic hardening model.

3. *S355 Steel (beam, constant)* was used for the wire elements This section uses all the properties of S355, with the only difference being the "isotropic" method was used to model the plastic hardening. This is due to the fact that wire elements cannot support a kinematic hardening which is part of the "combined" option used for the solid steel.

4. *S460 Steel (solid, homogenous)* was used for the welds. As stated previously, welds were only modeled on the Additional Web Panels; all other welded connections were modeled as Ties in ABAQUS, in order to simplify the model. The properties of S460 steel was used along with a "combined" plastic hardening effect.

Step Settings

To perform each investigation, a Dynamic Implicit analysis with Quasi-Static load application was executed on all of the models. The three steps used are termed as the Initial, Clamping, and Loading steps.

For the latter two steps where loads are applied, the Nonlinear Geometry option was turned on. Because the simulations will have high strains, it is important to use this option in the analysis. A Dynamic Implicit analysis was performed on each model using a Quasi-Static load application.

Interactions in ABAQUS

Four types of interactions are applied in these models, to simulate the different types of contacts which can be realized in a realistic joint configuration.

- *Surface-Surface Contact* – For parts which are bolted together, it is necessary to delineate this form of contact. In our models, the surface-to-surface interaction was characterized by defining both the normal and tangential behaviors of two connected elements. The normal behavior was defined as "hard contact," which negates the penetration of the slave surface into the master surface.

"Coulomb Friction" was used to determine the tangential behavior, in which we had two cases. For steel-on-steel contact, a friction coefficient of 0.4 was used; for aluminum-on-steel contact which characterized the friction pads, a friction coefficient of 0.53 was used. The latter value represents the 5% fractile for the dynamic friction coefficient between aluminum and steel, as discussed in D'Aniello et al, 2017.

Table III.4: Aluminum friction coefficients

	$\mu_{5\%}$	μ_{avg}	$\mu_{95\%}$
Friction Material M-1	0.53	0.59	0.64

The surface-to-surface interaction was used to define the bolt-hole contact, as well as the contact between the elements being connected by the bolts (ex: T-stub-column contact).

- *Tie Constraint* - Welds were not dimensioned in these models; the simplified version is to use the TIE interaction in ABAQUS to tie the welded elements together, ensuring there is no relative displacement between two instances along the interaction boundary. This kind of contact is used to represent full depth weld penetration. For nearly all of the welded elements this is an acceptable assumption along the whole contact surface, as the thickness of all these members are only 10mm. In these cases, the TIE interaction will closely resemble the actual behavior of the connection. The one exception to this rule was for the additional web panel of the column, whose contact surface with the column is much greater than 10mm. For this member, the outside 5mm edge of the whole panel was partitioned along the width and height; this area was modeled as the panel-column weld, as shown in Figure III.7.

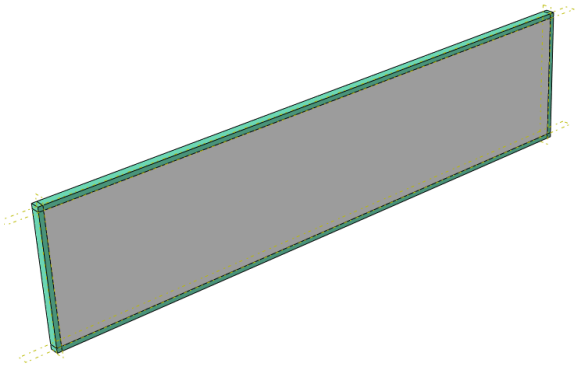

Figure III.7: AWP with equivalent welded area shown

- *Rigid Body* – Utilizing these types of interactions make it possible to define the behavior of the entire cross section or surface of an instance. By defining a reference point and assigning it to the proper surface, boundary conditions can later be established, as well as torsion controls and forced displacements, as shown in Figure III.9. The red area displays the column-base connection which is modeled as fully fixed.

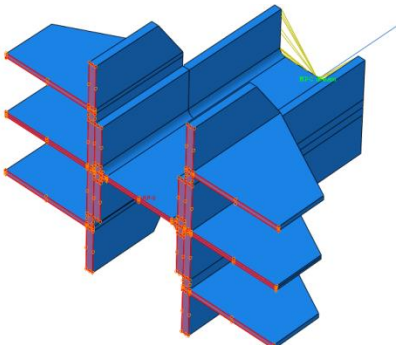

Figure III.9: Rigid Body interac

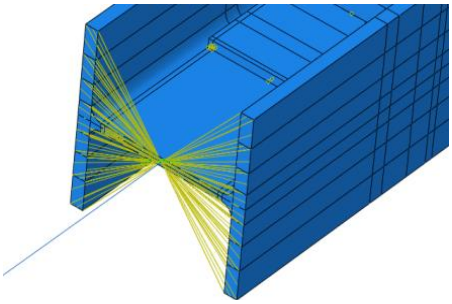

Figure III.8: MPC Beam Tie

- *MPC Beam* – Multi-point Constraints allow constraints to be imposed between different degrees of freedom in the model. Specifically in these models, it allows the one node at the end of the wire elements to be tied to the entire cross section of a beam/column. Figure III.8 gives a visual of the MPC Beam tie.

Application of Loads

During the loading step, the boundary conditions of the model were defined, along with the loading and amplitude of loading, and the intermediate torsional restraints on the beam.

Boundary Conditions

As previously stated, the boundary conditions were established at cross sections designated by Reference Points (RP). These points differ based on if the model is a full frame or a single joint.

- *Fixed Boundaries* – Points of fixity need to be established in the models. For joint models, this occurs at RP 1 and RP 2 in
- Figure III.10, which have all the translational degrees of freedom and the rotation around the axis of the column blocked.

  In the full frames, this boundary occurs at both column bases, which are fully restrained in all degrees of freedom.

- *Torsional Restraints* – In a real building, the main beams will be laterally and torsionally restrained by intermediate beams, and possibly by the concrete slab. In the ABAQUS models, this can be implemented by imposing torsional restraints at intermediate points along the beam, as displayed at RP 3.

  In the full frame, these occur at 1000mm intervals, starting from the beam-column node point. In the smaller models considering only one joint, the torsional restraints occur at 1000mm intervals, starting from the free beam end. The torsional restraints only restrict U2 and R1.

- *Load applied by Actuator* – In order to make the bending moment increase smoothly, it was decided to apply a displacement to the models instead of an actual force. In this way, the displacement can be restrained in the initial phase, while in the loading phase it will vary according to the imposed loading amplitude. For the joint models, the displacement was applied at RP 4 along the U3 degree of freedom.

  In the full frame model, the actuator was modeled as simultaneously acting on the external faces of both columns, as shown by the red areas. In these models the displacement was applied along the U1 degree of freedom.

  This forced displacement is characterized by either a monotonic or cyclic amplitude as described in the next section.

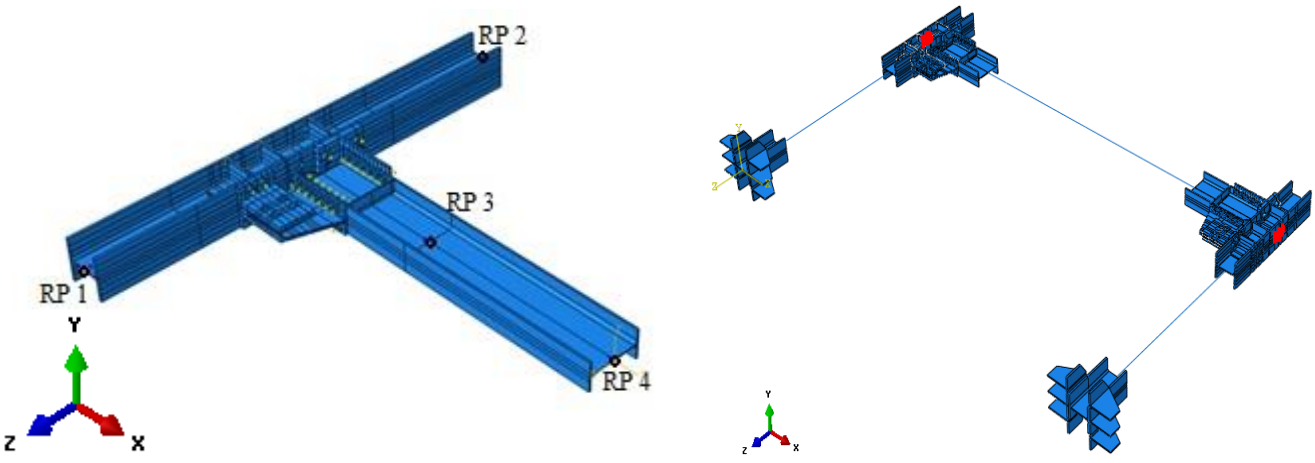

Figure III.10: Boundary conditions

Loading and Amplitude

Amplitudes were created for the application of loads on the models, to describe how each type of load is applied. Because we had models which were tested under either monotonic or cyclic loading, it was necessary to define three amplitudes: Bolt Clamping, Monotonic Loading, and Cyclic Loading.

- *Bolt Clamping* – applied in a Time Period of 0 to 1 second, with a linearly increasing amplitude from 0→1 over 1 second

- *Monotonic Loading* – a Time Period of 0 to 102000 seconds was used with a linearly increasing amplitude from 0→1 over the entire time period, as shown in Figure III.11.

- *Cyclic Loading* – defined by AISC protocol from the ANSI/AISC seismic provisions for buildings. The cyclic loading can be viewed in Figure III.11 and was defined with a Time Period of 0 to 102000 seconds.

Both loading cases have a maximum number of increments set to $1*10^{6}$, with an initial increment size of 0.01 and a minimum increment size of $1*10^{-15}$.

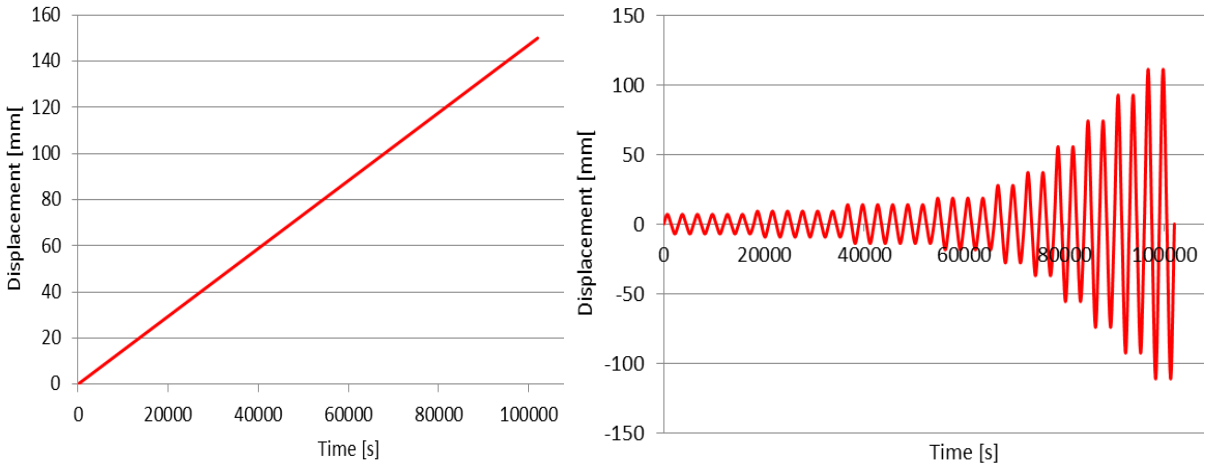

Figure III.11: LEFT- Monotonic loading amplitude; RIGHT - AISC cyclic loading amplitude

Bolt Loads

The pretension force applied to the bolts has a significant effect on the seismic behavior of the FREEDAM joint. Not only are the bolted connections a significant aspect of the joint, but the slip force of the friction joint is proportional to the strength of the clamping force, as discussed in D'Aniello et al, 2017. The bolts are all pretensioned, with the amount of pretension based on the cross sectional area of each bolt as described by the following equation:

$$F_b = 0.7 \cdot f_u A_{eff,b}$$

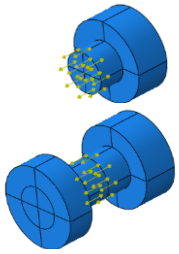

Figure III.12: Bolt load applic

The amount of pretension used for each bolt class was discussed previously in Table III.3: Bolt pretension force, which was applied by using the predefined "Bolt load" option in ABAQUS. The bolt loads were applied to the approximate center of the bolt shank cross section along the axis of the bolt. In the Clamping phase, the bolts were subjected to an applied force corresponding to their above strengths. In the Loading phase, the bolt load was modified to be "fixed at current length".

The bolts connecting the L-stubs to the haunch functioned as the clamping mechanism for the friction damping device. As the slip force (and thus the dissipative capabilities) of the joint is proportionally dependent to the pretension force in the bolts, this parameter needs to be tightly controlled.

3.2 Other Modeling Assumptions

4.2.1 Typical Joint dimensions

The geometry of the ABAQUS models for the parametric analysis is detailed by the sub-structuring shown in Figure III.13. Half of the bay length was used for the beam, and one half of the column height in either direction of the joint was used. Lateral torsional restraints were used every 1000 mm, which is the spacing of the secondary beams perpendicular to the plane shown.

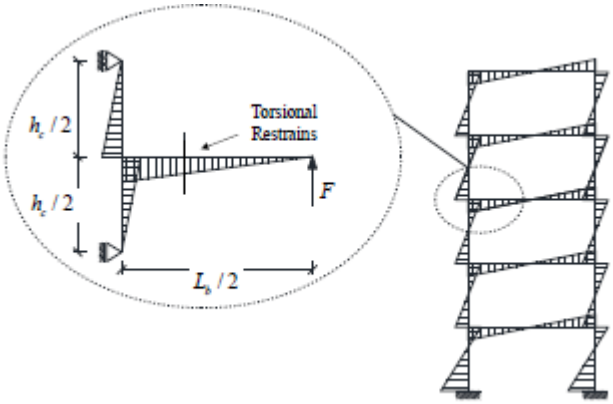

Figure III.13: Substructure of ABAQUS model; D'Aniello et al. 2017

4.2.2 Modeling of Column base

The column-base connection was modeled with the appropriate flange stiffeners, and therefore it was assumed that the base has sufficient stiffness that we did not need to model the base plate or any element further down.

4.2.3 Geometry for the consideration of wire elements

For this project, each individual part was modeled as either a solid or a wire element. All of the critical components of the joint were modeled using solids, while the wire elements were utilized in the full frame models for sections of the members that were a significant distance away from each joint. The verification for using wire elements was discussed previously.

In the case of the columns, the column-wire elements started at a vertical distance of $b_{f,col}$ away from the end of the closest joint component. For the FD joint, the closest component was considered as the T/L-stub; for RBS joint, the closest component was considered as the extended end plate. In the case of beams, the beam-wire element started at a distance of $2 * b_{f,beam}$ away from the closest critical joint component.

Table III.5: Wire distance from joint

Section	Distance from joint	Distance [mm]
IPE270	$2 \cdot b_{f,beam}$	270
HE200B	$b_{f,col}$	200

For the FD joint, the closest component was considered as the edge of the beam flange stiffener applied at the end of the haunch; for the RBS joint, this distance was considered as the location of the beam-beam splice.

3.3 Output from ABAQUS

From ABAQUS, we can extract certain parameters from the output file after the analysis has been completed. From the rigid bodies where the displacement is applied to the model, it is possible to obtain the reaction force in the direction of displacement application as well as the displacement with respect to time. For the single joint models, the displacement was applied vertically, along the z-axis. Therefore, reaction force and displacement were obtained at the free end of the beam along this same axis. For the full frame models, the displacement was applied at each story at the external face of the column; therefore, the reaction force and displacement was also taken in this direction. Considering the length of the lever arm of the beam, it is possible to then calculate the bending moment as a function of beam length and shear force. Also considering the lever arm and displacement, it is possible to calculate the interstory drift/joint rotation.

While these few parameters represent the response of the joint overall, it is also necessary to understand the behavior at the level of the friction damping device for the FD joints. To do this, the vertical displacement was taken at the lower edge of the haunch. After measuring the moment arm of the damper (taken as vertical distance from the center of the slip surface to the center of the T-stub), it is possible to calculate the rotation of the damper.

In the RBS MRF frames, it is also possible to obtain the internal moment of the joint. This was done by making a free body cut at the center of the dog-bone section, and extracting the bending moment around the beam's strong axis.

Other output from ABAQUS includes screenshots of the model's deformed shape, the Von Mises stresses, and PEEQ. Von Mises stresses are a scalar representation of the combined stresses along the three major axes inside a material.

$$\left(\frac{(\sigma_1-\sigma_2)^2+(\sigma_2-\sigma_3)^2+(\sigma_3-\sigma_1)^2}{2}\right)^{0.5}=\sigma_v$$

$$\sigma_v \geq \sigma_y$$

Where σ_1, σ_2, and σ_3 are unidirectional stresses along the three major axes, and σ_v is the Von Mises stress. As a failure criterion, it is simple for an engineer to check whether the induced Von Mises stress will exceed the material yield strength, thus causing the material to nonlinearly deform.

Another parameter utilized in FEM is PEEQ (Plastic Strain Equivalent). This is another scalar value which measures all of the components of plastic strain at each position in the model. ABAQUS user's manual defines the PEEQ as:

$$\bar{\varepsilon}^{pl}|_0+\int_0^t \dot{\bar{\varepsilon}}^{pl}dt$$

Where $\bar{\varepsilon}^{pl}|_0$ is the initial equivalent plastic strain, and $\dot{\bar{\varepsilon}}^{pl}$ depends on the model. For classical metal plasticity:

$$\dot{\bar{\varepsilon}}^{pl}=\sqrt{\frac{2}{3}\dot{\varepsilon}^{pl}:\dot{\varepsilon}^{pl}}$$

PEEQ is important for determining which parts of the model can be expressed as experiencing plastic deformation.

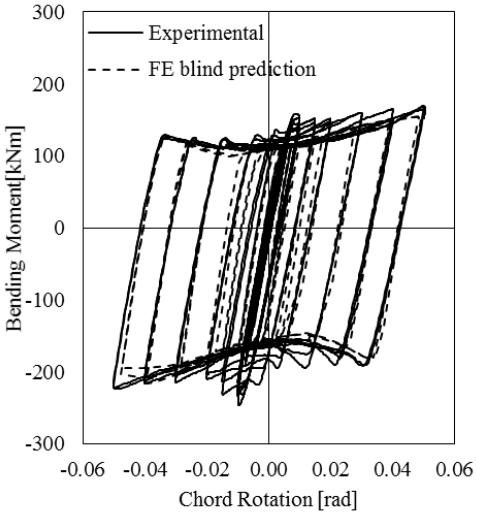

a) Configuration 1

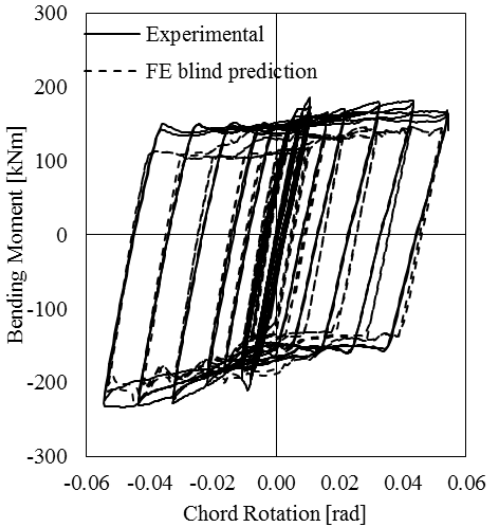

b)) Configuration 2

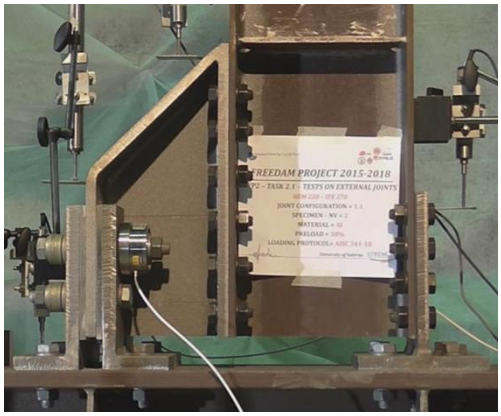

a) Experimental joint FD 1-1

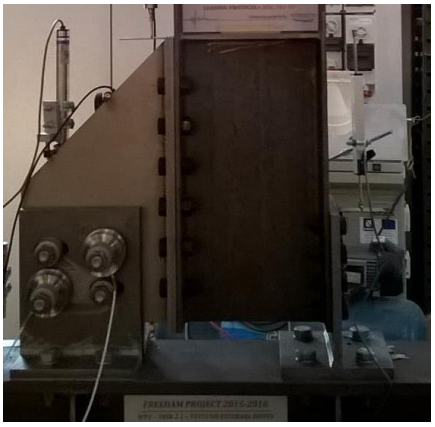

b) Experimental joint FD 2-1

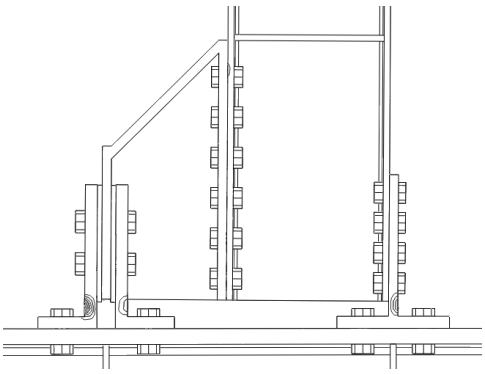

c) PEEQ distribution for model FD 1-1

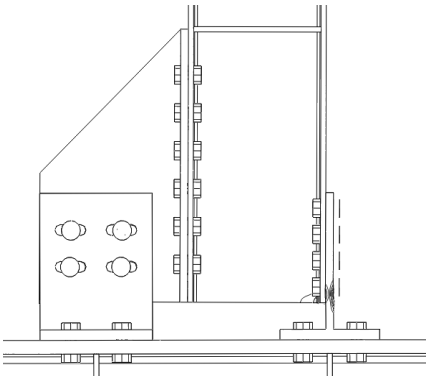

d) PEEQ distribution for model FD 2-1

Figure III.14: Calibration of FD models form experimental results, (D'Aniello, Zimbru and Latour)

Chapter IV: PARAMETRIC ANALYSIS

4.1 Configurations of FD Joint Typologies

In the investigation of friction damping joints, out of the two parent FREEDAM joint configurations, FD2 was chosen for the main body of this parametric study. As explained previously, this joint configuration is easier to assemble and it has a more symmetric hysteric response than FD1. Also, in the near future FD2 will be implemented in a full frame mock-up. The possibility of comparing theoretical results from this paper and the empirical results from the future test is another reason why FD2 was selected for this thesis. Both configurations realize a friction damping device, with the main difference being the orientation of the slip surface and of the L-stubs. Below is shown a visual comparison of both parent configurations of the FD beam-column connection: FD1 and FD2 (configuration 1 and 2 respectively).

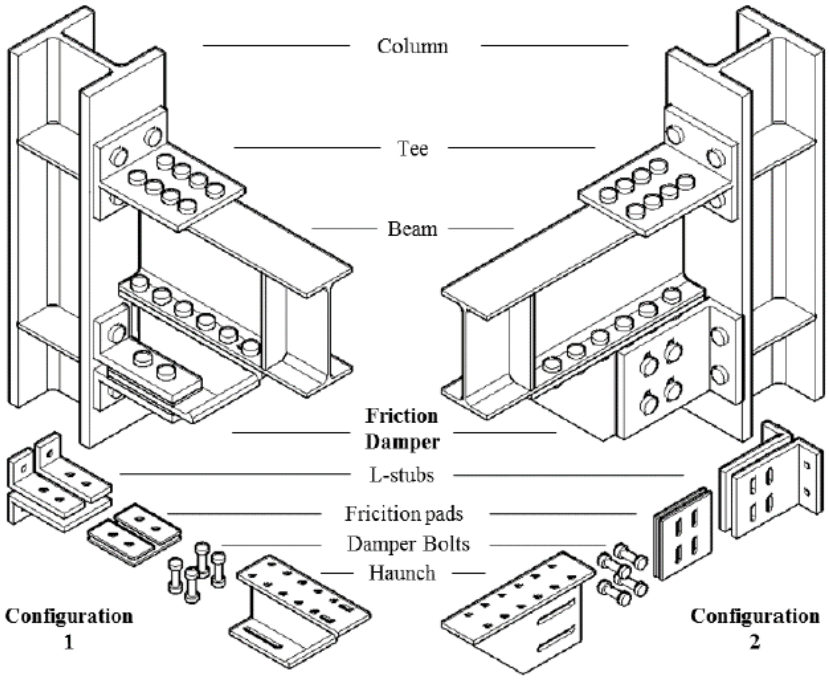

Figure IV.1: FREEDAM joint configurations

Different sub-configurations can be made from these two connections by altering the geometry of the components. This can be done by altering the elements in the friction device, for example by enlarging the elements, adding more bolts, changing the bolt clamping force, etc. From these sub-configurations, different assembly types can be realized, only by changing the type of beam

and column used. For this paper, mostly FD2 was tested using different sub-configurations and assemblies.

4.2 Verification for the use of wire elements in full frame analysis

For the FREEDAM FEM analysis, two full scale 1bay-2story models were created in ABAQUS to compare the response of frames with RBS to frames with FREEDAM joints. In order to simplify the analysis, wire elements with properties of the beams/columns were used at the intermediate points in the model. A theoretical comparison was performed to verify that these models with wire elements would have a similar response to the models with all solid elements. These wire parts were assigned in ABAQUS to have the same geometric and material properties as the beams and columns that they were replacing, and were tied to solid elements by the use of an MPC Beam. For this test, a single joint was modeled using solid elements for the joint components, while the wire elements were used at a safe distance away from the joint components (explained in Chapter III), so as to not have an impact on the overall response of the system. The purpose of experimenting with wires is to reduce the number of finite elements in the full frame model.

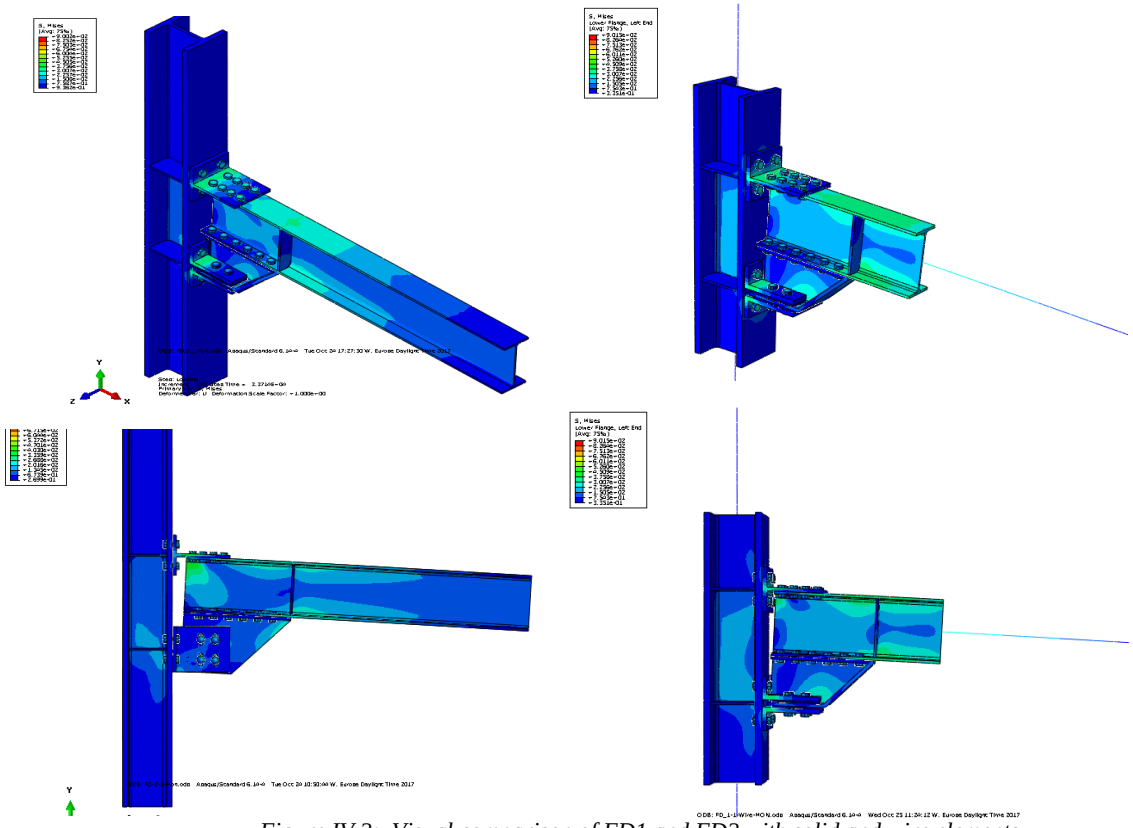

Figure IV.2: Visual comparison of FD1 and FD2 with solid and wire elements

Two joint configurations were compared for this verification: FD1-1 and FD2-1. In this case, it is most critical to view the behavior of the joint using the full chord length, as this will give us an idea of the behavior of solid compared to wire elements. For each joint, the column and beam lengths will remain the same: 2000mm for the column, and 1865mm for the beam (measured from beam free end to centerline of column). In the first model of each configuration, these elements will be composed only of solid elements. For the second model, the solid elements will extend a certain distance away from the friction damping device; past this distance, wire elements will be tied to the solid elements in order to simulate a full joint.

The bending moment was evaluated based on the reaction force measured at the point of application of the displacement history multiplied with the distance to the central axis of the column, while the chord rotation is calculated by obtaining the displacement at the beam tip divided by the distance to the column axis.

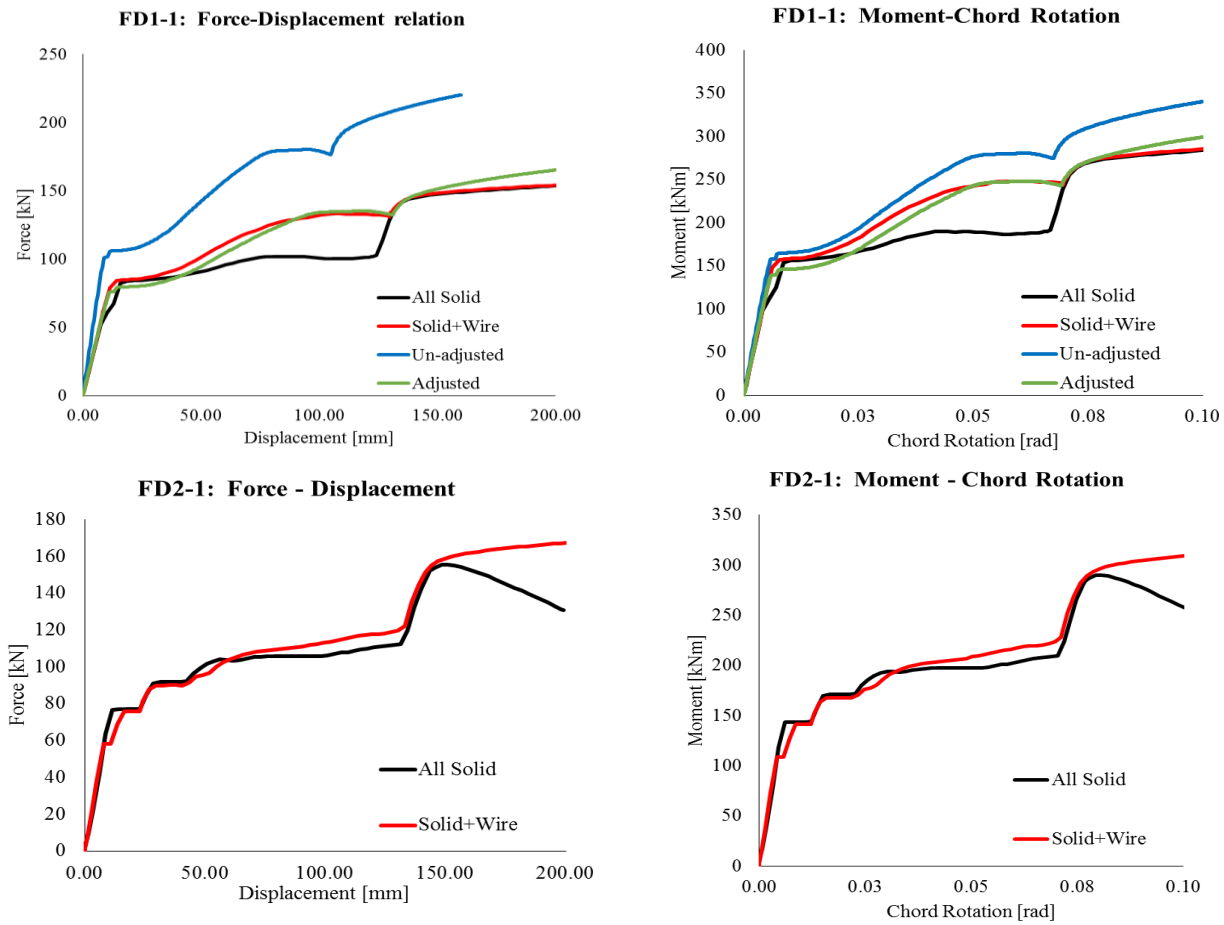

Figure IV.3: Results from the experimental comparisons of solid to solid+wire models

The joints have different behavior post-slip. From Figure IV.3, it can be seen that FD1-1 has a higher capacity in hogging moment and is characterized by a smooth, nonplanar response in the post-slip region. FD2-1 has a lower capacity in hogging than FD1-1, and is characterized by a saw-toothed shape, planar response after slipping occurs. For the analysis of FD1-1, there was an error in the behavior of the All-solid model; therefore, another model of the same configuration type and assembly size was used, which had been analyzed with a different clamping force (Un-adjusted model). Because the model geometry was the same and we know that bolt clamping force has a linearly scaling effect on FD joint bending moment capacity, a simple coefficient of 0.75 was applied to the results from the un-adjusted model in order to obtain a new curve (Adjusted model). These curves were used to determine whether or not the results from the models with solid+wire elements were a good fit for the all-solid model.

Considering a max of 0.05 rads chord rotation, the variation in bending moment capacity is negligible at 5% and 8% for FD1 and FD2 respectively. After this standard limit, the only large variation is after 0.08 radians of rotation, which is beyond what any structure should experience. Possibly this is due to how the bolt clamping force was defined in the model; however, this deviation is encountered only after large rotation and can be neglected. From these results, it was deemed that wire elements can be implemented into full frame models.

4.3 Full frame analysis: RBS vs. FREEDAM

An important step in the creation of FREEDAM joints is the comparison with a standard moment resisting joint currently used in building construction. Current seismic resistant joints designed

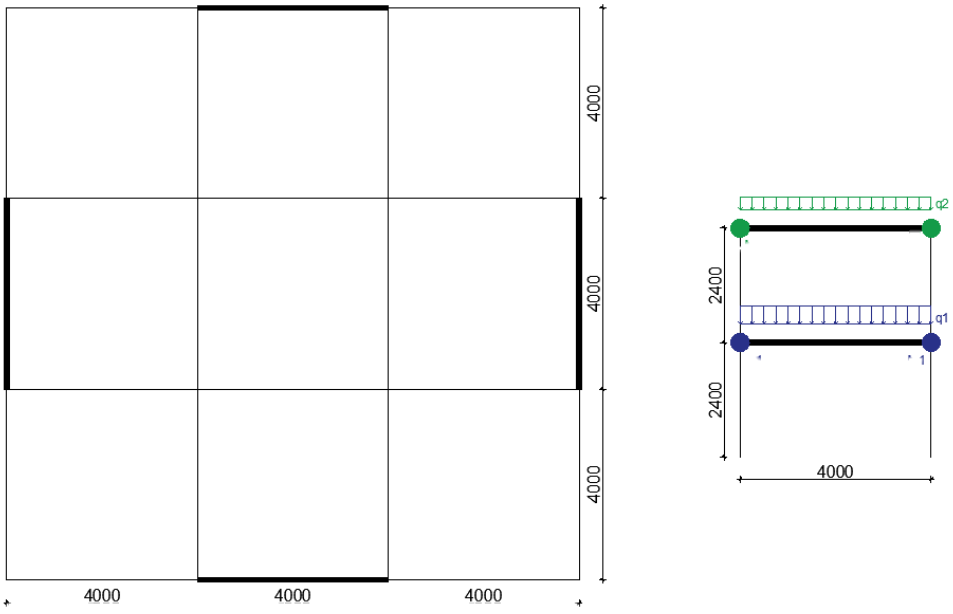

Figure IV.4: Full frame layout and gravity loading

from Eurocodes are based off of the Capacity Design principle. In these designs, either the joint

or beam is created to be significantly weaker than the columns. This is to ensure that plastic hinges may form in these areas, rather than in the columns which are the most critical elements of the building. To effectively compare the responses of FD joints to a standard RBS joint, some full frame models were compared. These models include comparing two frames, the first with one bay and one story, the second with one bay and two stories. These two frames were modeled first with typical RBS MRF joints, and after with FD MRF joints. XXXcheck loading Gk

One joint which is typically used in Capacity Design is the RBS joint, where the beam cross section is strategically reduced in one area a certain distance away from the joint. This is where the plastic hinge is meant to form, away from the column face, in the case of strong seismic actions. In order to examine the plausibility and effectiveness of FD joints compared to modern moment resisting joint, a comparison of full frame analyses is required. Thus, the responses of one and two story models utilizing first RBS MR joints and then FD joints were compared. The frames were modeled with HEB200 sections as columns and IPE270 sections for beams.

The comparison of joints can be seen in Figure IV.5.

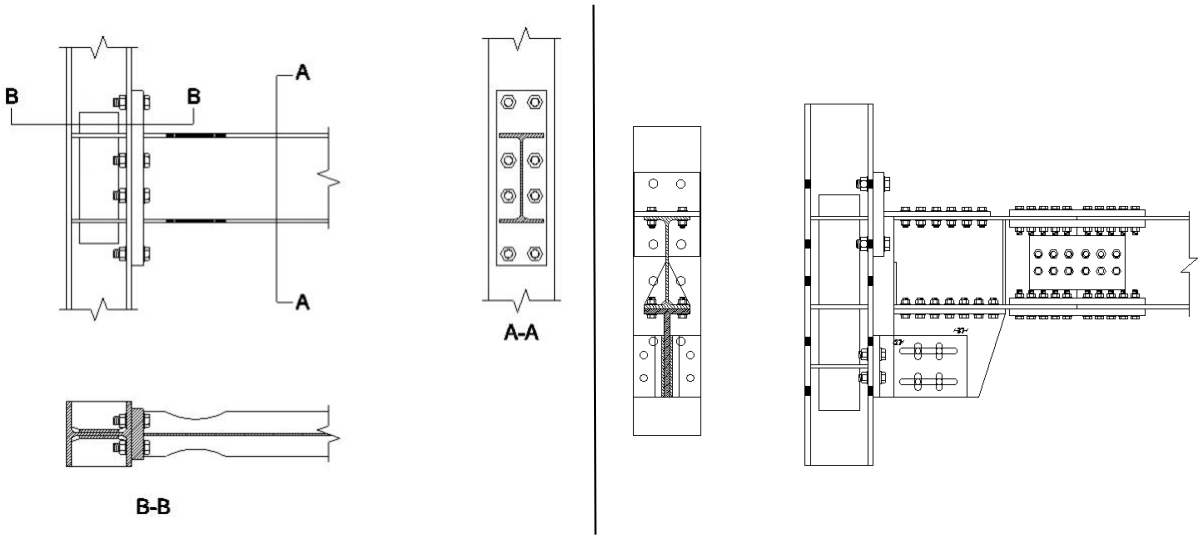

Figure IV.5: LEFT - Drawing of RBS joint; RIGHT - Drawing of FREEDAM joint

When running a large scale analysis, it is important to understand the full scope of impacts from the effects of progressive material damage, from geometrical imperfections, and from gravity loads. In order to achieve this, we ran tests using all of these parameters while changing the coefficients. These parametric analyses were performed on the RBS frames, to see variables would have a significant impact.

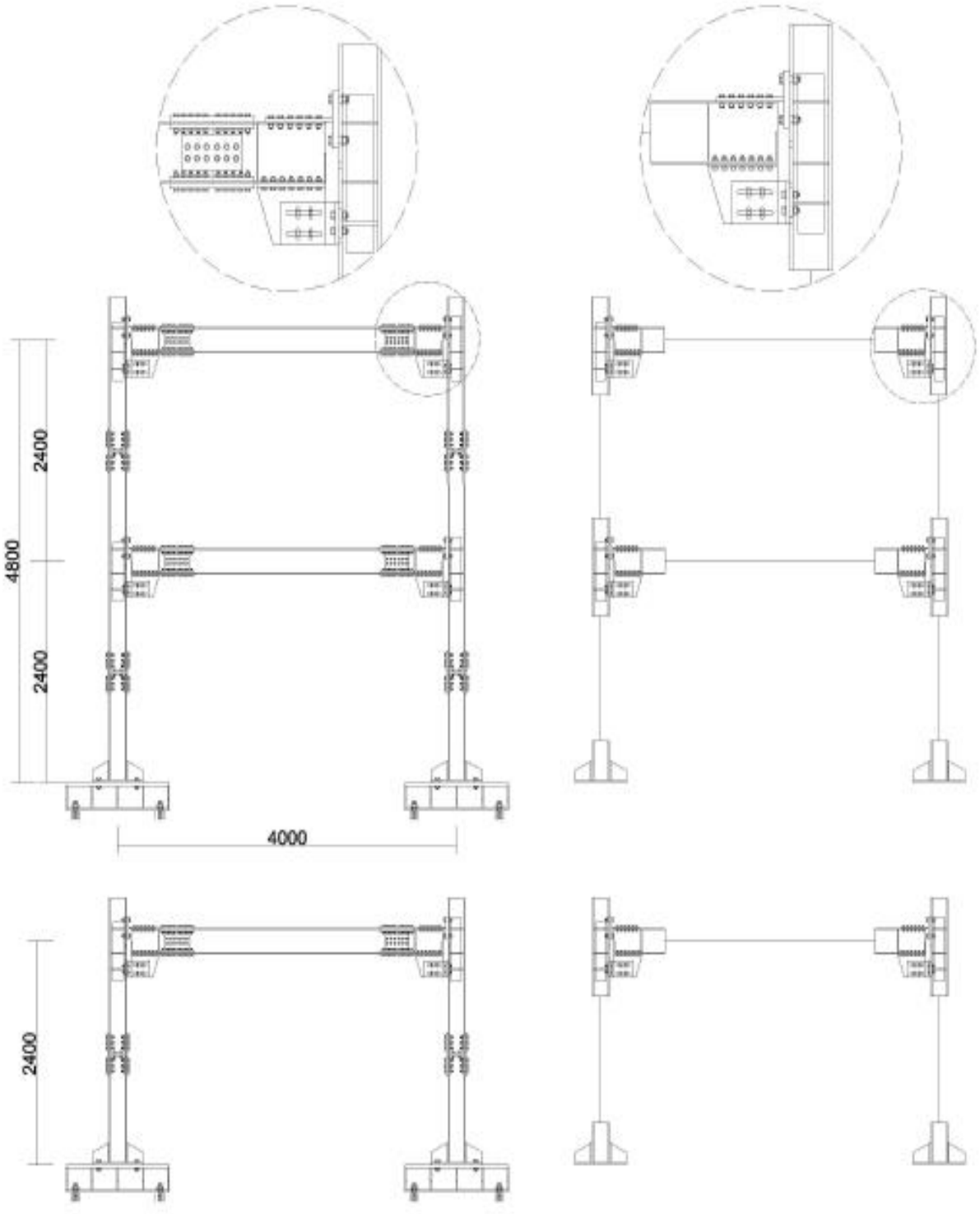

Figure IV.6: LEFT - Experiemental FD MRF frame; RIGHT - ABAQUS models of 1 and 2 story FD MRF frames

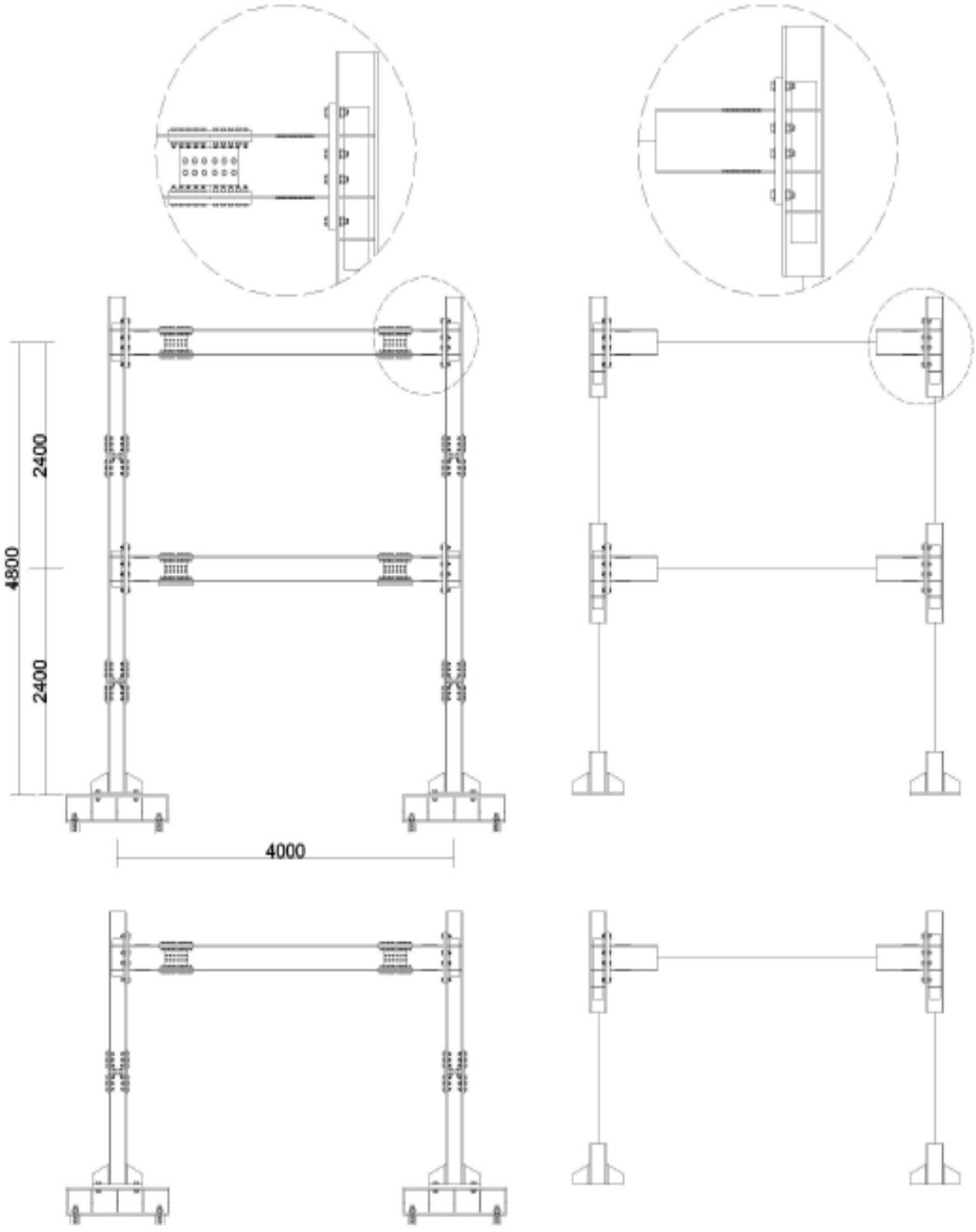

Figure IV.7: LEFT – Experimental RBS frames; RIGHT – ABAQUS RBS frame models

4.3.1 Modelling material damage

In ABAQUS it is possible to model progressive material damage and failure in engineering structures. In a real material after yielding, damage occurs in which the material properties are permanently altered which affect both the plastic and elastic behavior. It is accepted that moderate to high stress triaxiality leads to accelerated structural degredation during plastic deformations. Complete material failure refers to the loss of load carry capacity that results from the progressive degradation of material stiffness.

Two distinct types of material failure can be implemented in order to predict a more accurate response. These failures are void nucleation and growth, and shear band localization, as shown in Figure . For the full frame models, only void nucleation was considered through ductile material damage initiation.

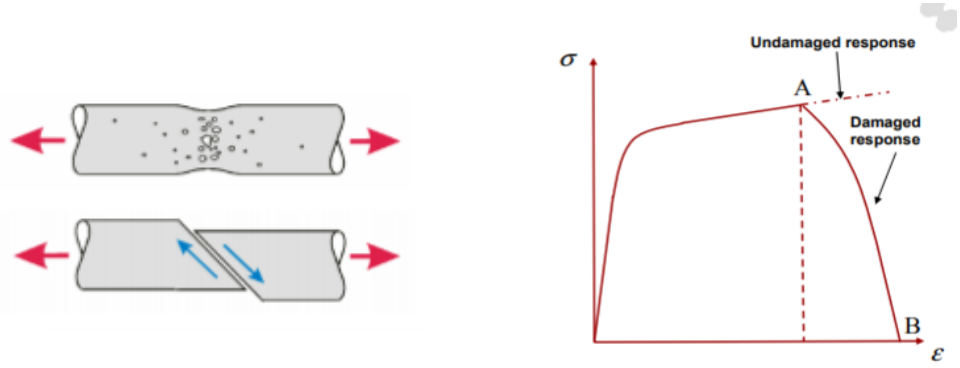

Figure IV.8: LEFT - Void nucleation and shear banding; RIGHT - Undamaged vs damaged materi

Material damage can be implemented in ABAQUS through editing of the input file. The model assumes that the equivalent plastic strain (PEEQ) at the onset of damge is a function of stress triaxiality and strain rate, where stress triaxality can be determined from the following equation:

$$\eta = -p/q$$

Where η is the stress triaxality, p is the pressure stress and q is the Mises stress. The same material damage initiation was used for all of the materials and can be viewed in Table IV.1.

Table IV.1: Stress triaxiality

Ductile Damage

Fracture strain	Stress Triaxiality	Strain rate
20	0	0.001
14.0752	0.0667	0.001
9.9102	0.1333	0.001
6.9847	0.2	0.001
4.9326	0.2667	0.001
3.4969	0.3333	0.001
2.4988	0.4	0.001
1.8132	0.4667	0.001
1.3543	0.5333	0.001
1.0645	0.6	0.001
0.908	0.6667	0.001
0.8646	0.7301	0.001
1.0576	0.851	0.001
20	0	250
14.0752	0.0667	250
9.9102	0.1333	250
6.9847	0.2	250
4.9326	0.2667	250
3.4969	0.3333	250
2.4988	0.4	250
1.8132	0.4667	250
1.3543	0.5333	250
1.0645	0.6	250
0.908	0.6667	250
0.8646	0.7301	250
1.0576	0.851	250

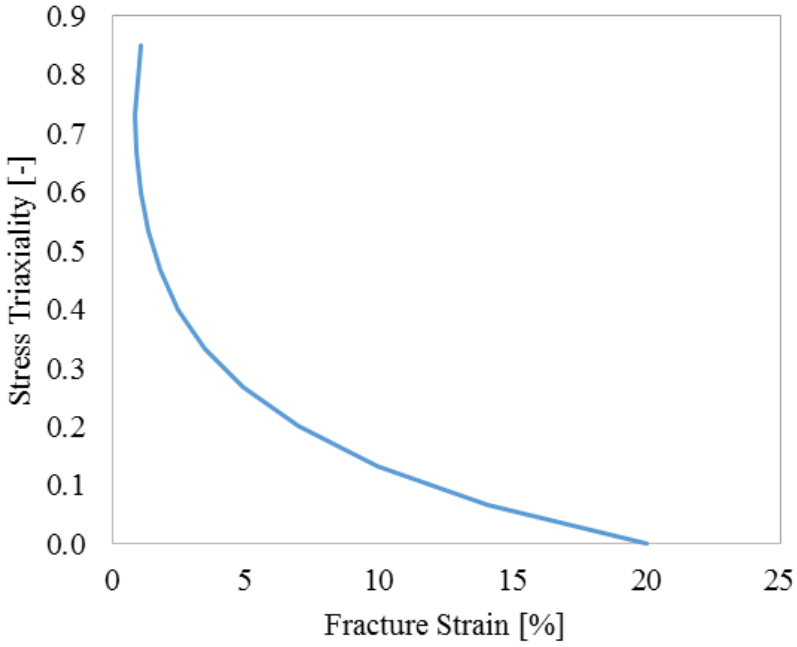

With these values, static nonlinear analyses were performed to verify whether the damage plays a significant role in structural response and if the damage model is a good fit for our analysis. A comparison of different material damage coefficients was performed for coefficients of 0, 0.1, and 1. Along with this, one analysis was performed with gravity loads.

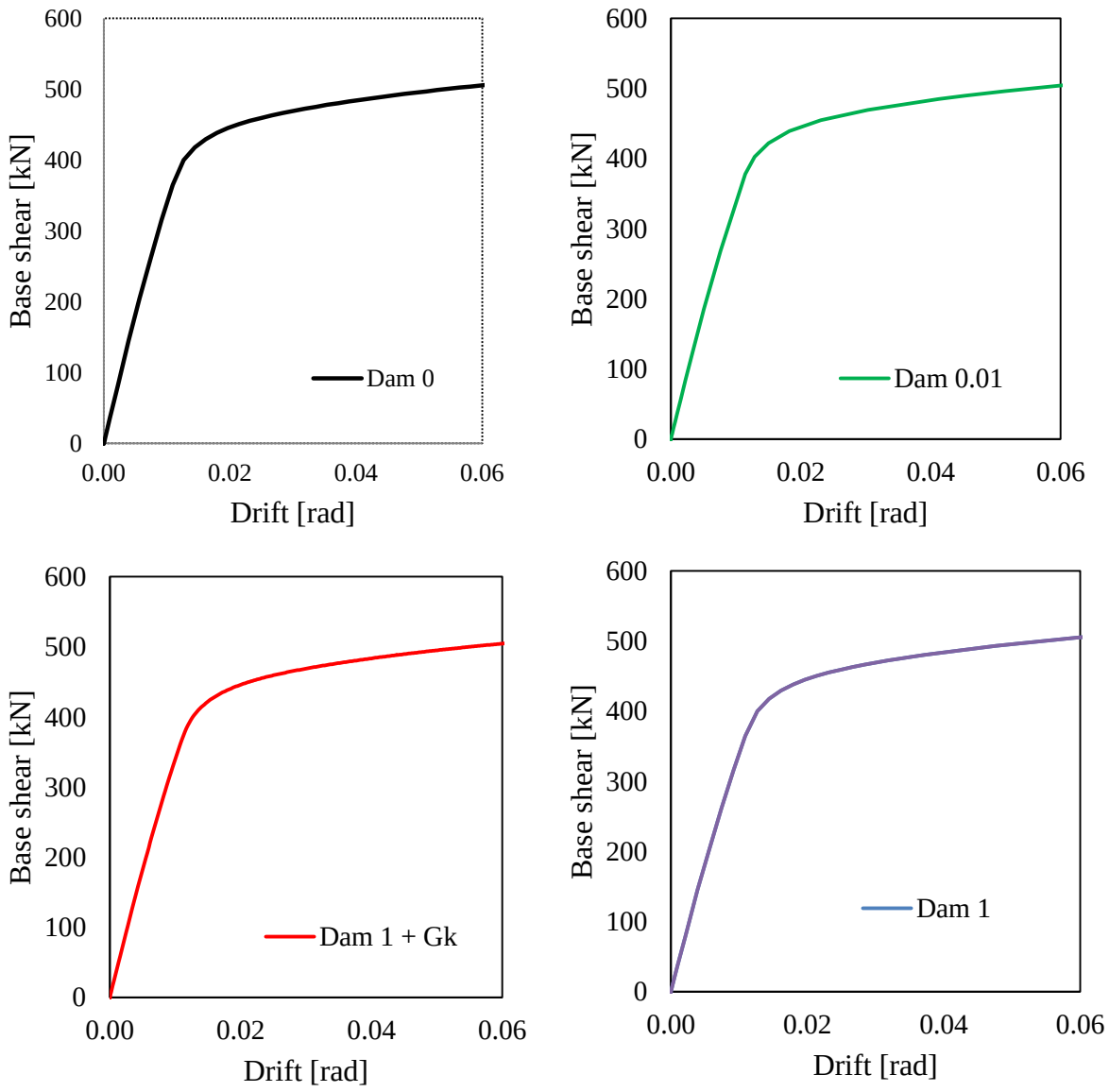

Figure IV.9: Comparison of material damage coefficients

The figures above tend to show that no matter what damage is applied to the structure, there is in fact no significant effect on the structural response. While material damage is important to model on the full structural analysis, these results suggests that the damage model is not a good fit for this structure. The following graphs and images show the compilation of base shears and bending moment resistance, as well as PEEQ and Von Mises stresses. Because the responses of all the static pushover analyses were the same, the images from the zero damage analysis can be used to represent all.

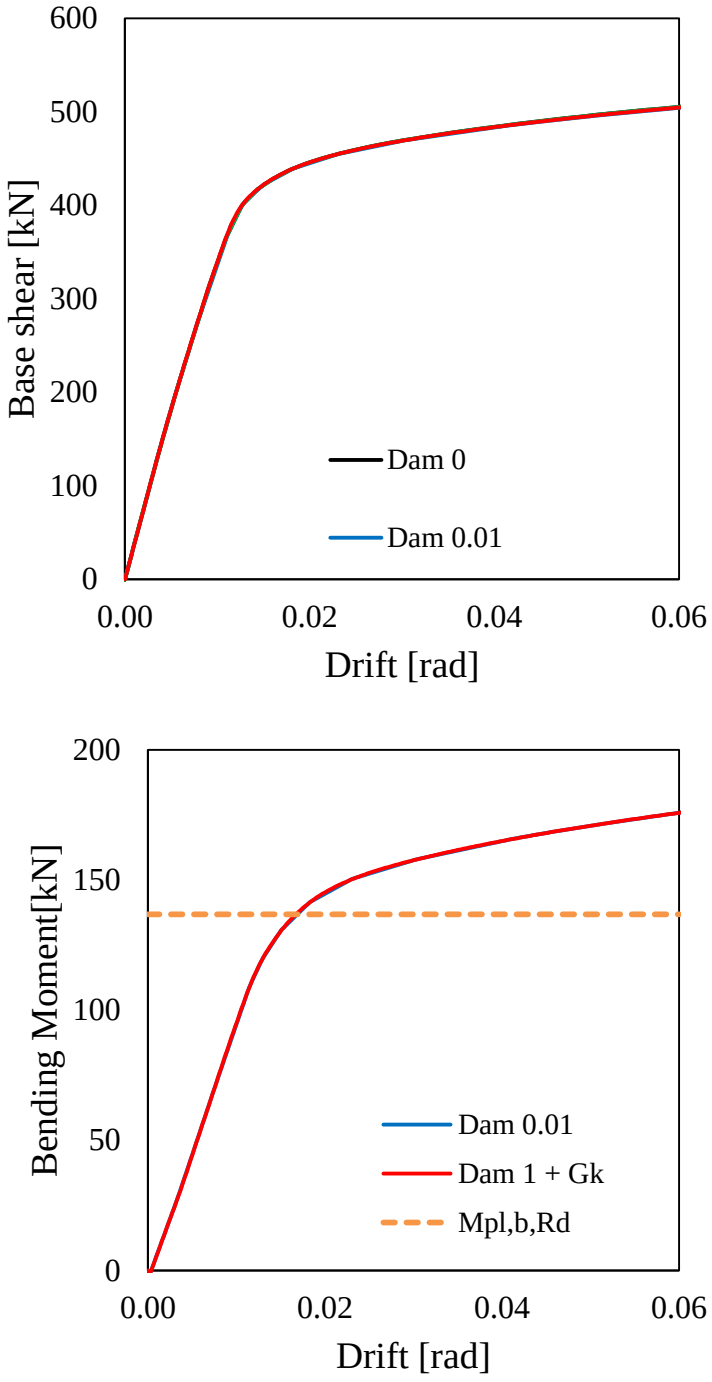

Figure IV.10: TOP - Base shear vs drift; BOTTOM - Bending Moment vs drif

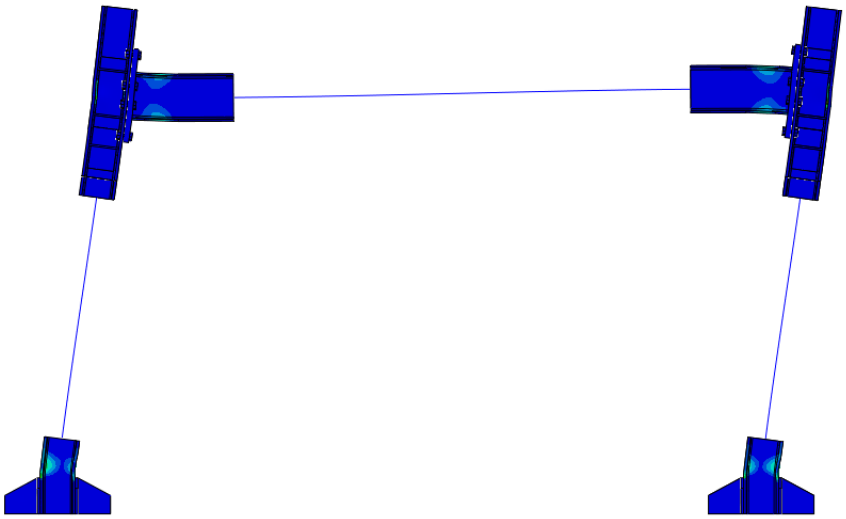

Figure IV.11: Deformed shape of single story RBS frame

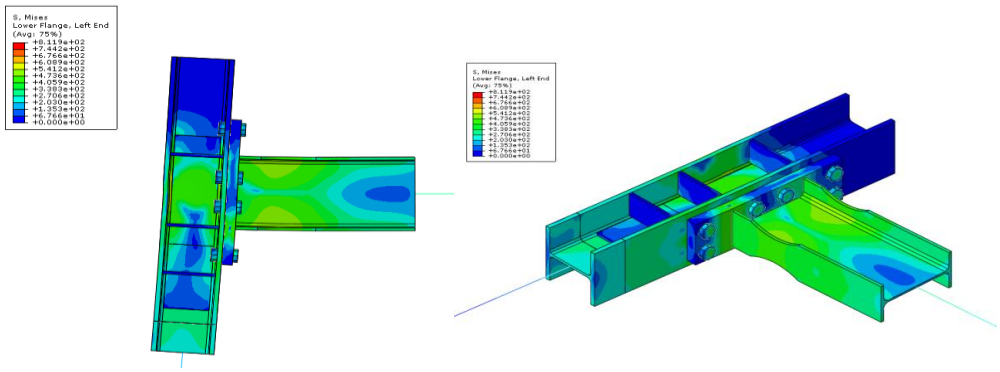

Figure IV.12: Von Mises stresses

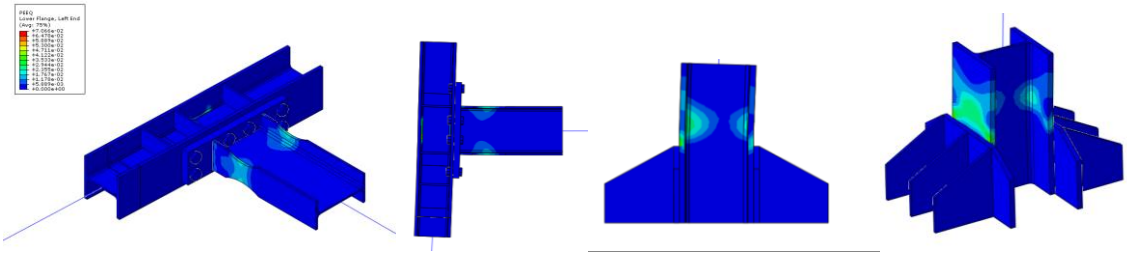

Figure IV.13: ABOVE - PEEQ at 2% interstory drift, joint and column base; BELOW – PEEQ at 4% drift

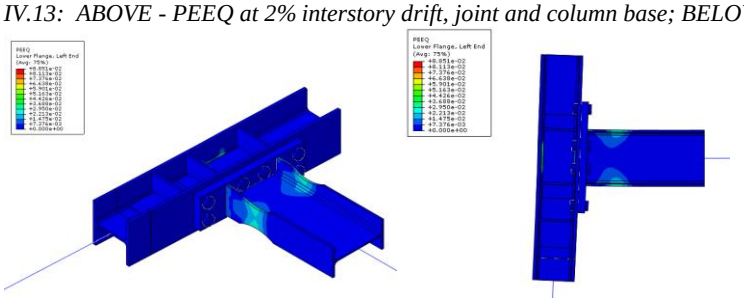

4.3.2 Imperfection

The modelling of initial geometrical imperfections is important for structural analysis to be conservative, as any irregularities can reduce the load carrying capacity and make it more susceptible to buckling. For IPE270 with a beam flange width of 135mm, the out-of-square-imperfections should be taken as 2.7 mm, as calculated from the Eurocodes.

Table IV.2: Out-of-square tolerances for IPE sections (Arcelor Mittal)

Falta de paralelismo / Out-of-square / Fuori squadra — k+k' (mm) [in.] 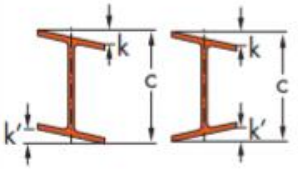	b ≤ 110mm	1.5 mm
	b > 110mm	0.02b mm (max 6.5mm)

To model such imperfections in ABAQUS, a buckling analysis was first performed on the frame to determine buckling modes. The modes were selected in which each flange of the RBS cross section was buckling, one mode per beam per flange. This was done in order to mimic the out-of-scquare imperfection for beam flanges. The modes can be easily input into ABAQUS input file with the following code, which shows the four buckling modes and imperfections we selected for the one story frame. The following figure shows the input of imperfections using the mode number corresponding to flange buckling, as well as the coefficient of the imperfection.

```
*IMPERFECTION, FILE=Buckling, STEP=1
15, 2
16, 2
21, -2
22, -2
```

Figure IV.14: Imperfection input for ABAQUS file

The effects of imperfections were examined on the RBS frame, primarily on the one story model. In order to make an accurate comparison, models were assigned with different coefficients of the imperfections obtained from the buckling modes. The coefficients tested are 0, 1, 2, -2, -4, and -4 inverse. The positive coefficients represent when the imperfections are modelled according to the buckling mode. The negative coefficients represent when the imperfections on one side of the beam are reversed (as seen in Figure IV.14, and the negative inverse coefficient represent when imperfections on the other side of the beam are reversed.

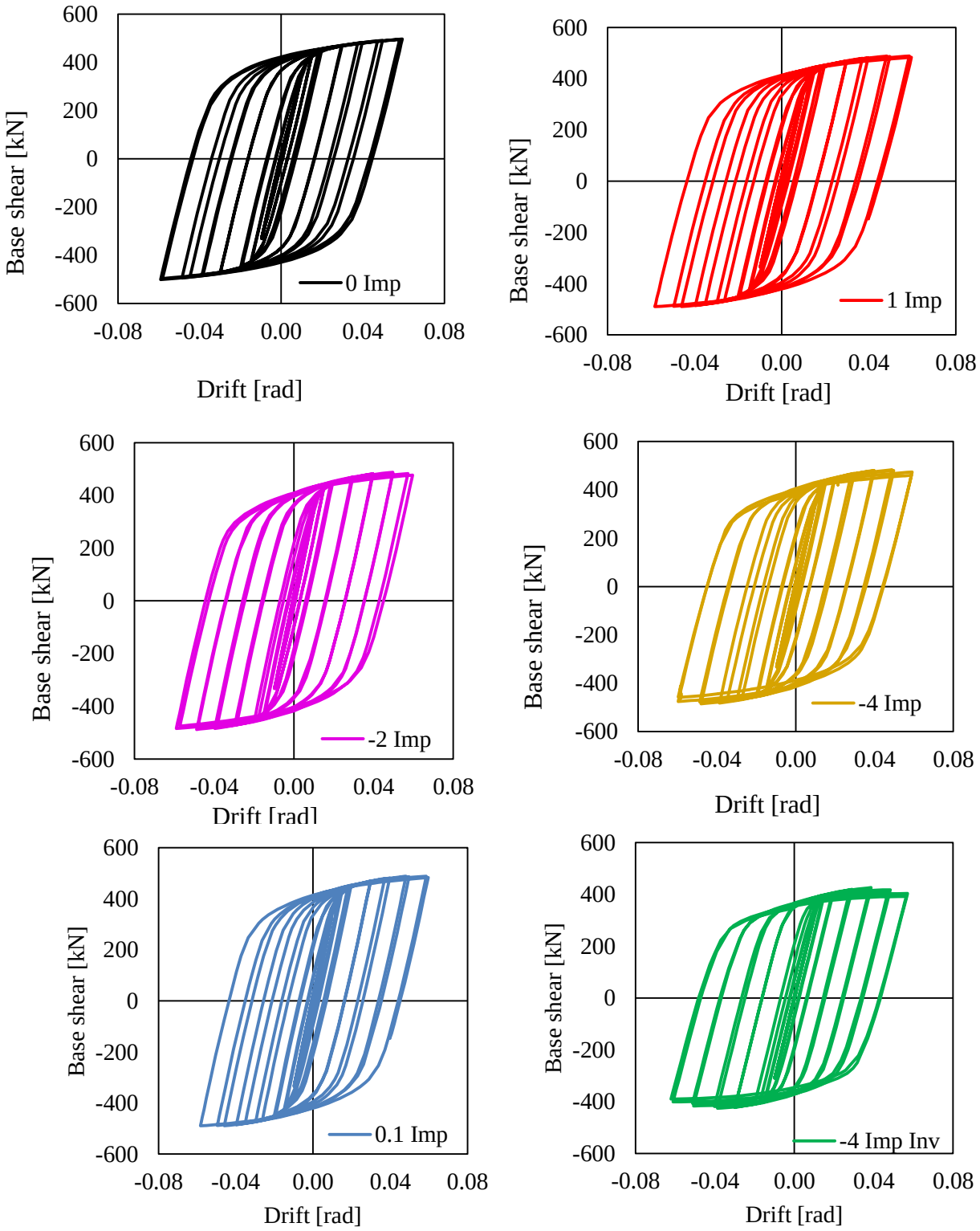

Figure IV.15: Imperfection calibration

Cyclic analyses were performed on the models using the AISC loading protocol. The following table and figures show the base shear compared to drift rotation for these analyses with different factors of imperfections.

The imperfections make a noticeable difference in the cyclic behavior of the model. The graph with 0 imperfections displays a very regular hysteric loop, with the max base shear perfectly following the shape of the static pushover curve. As the imperfections increase, there is an increasingly irregular hysteric shape as the base shear deteriorates after each cycle.

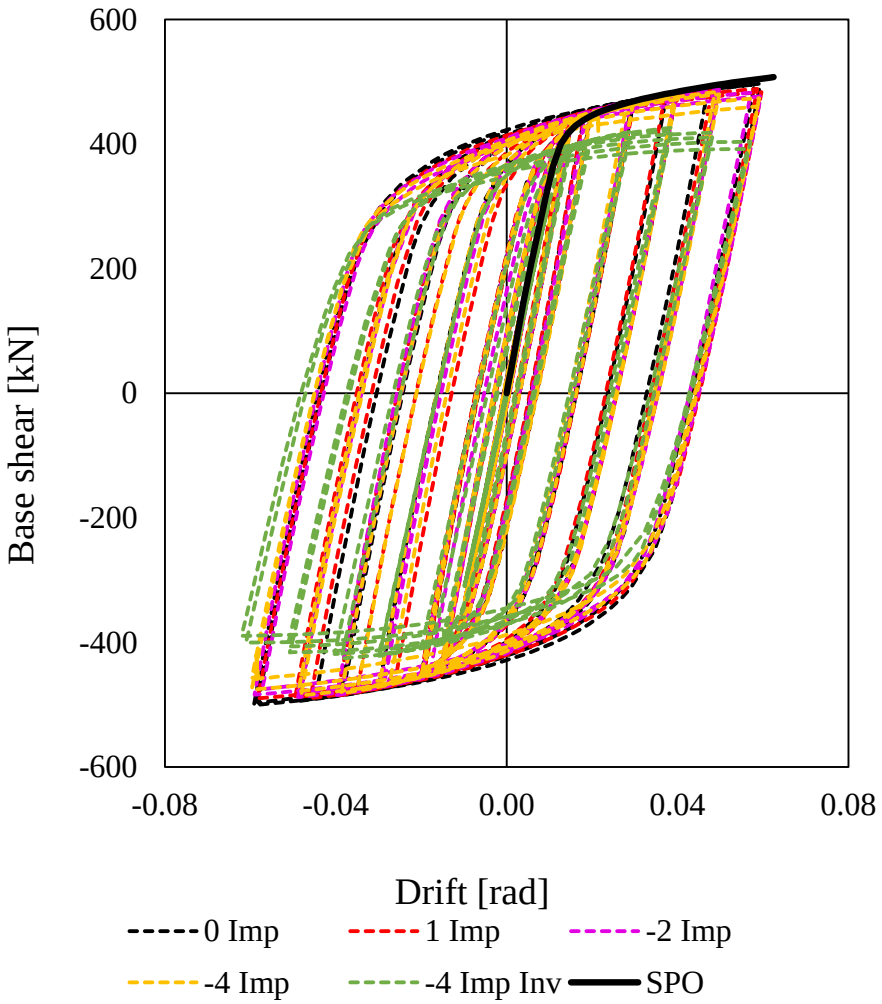

Figure IV.17: Use of dynamic nonlinear analysis to compare imperfections

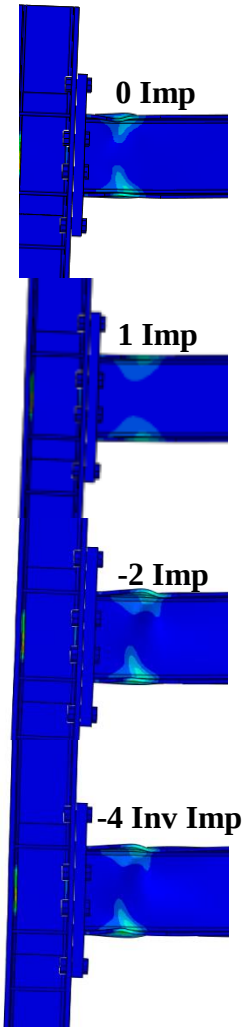

Figure IV.16: PEEQ @ 4 drift

While the base shear shows the lateral forces on the column base, it is also important to examine the bending moment in the beam.

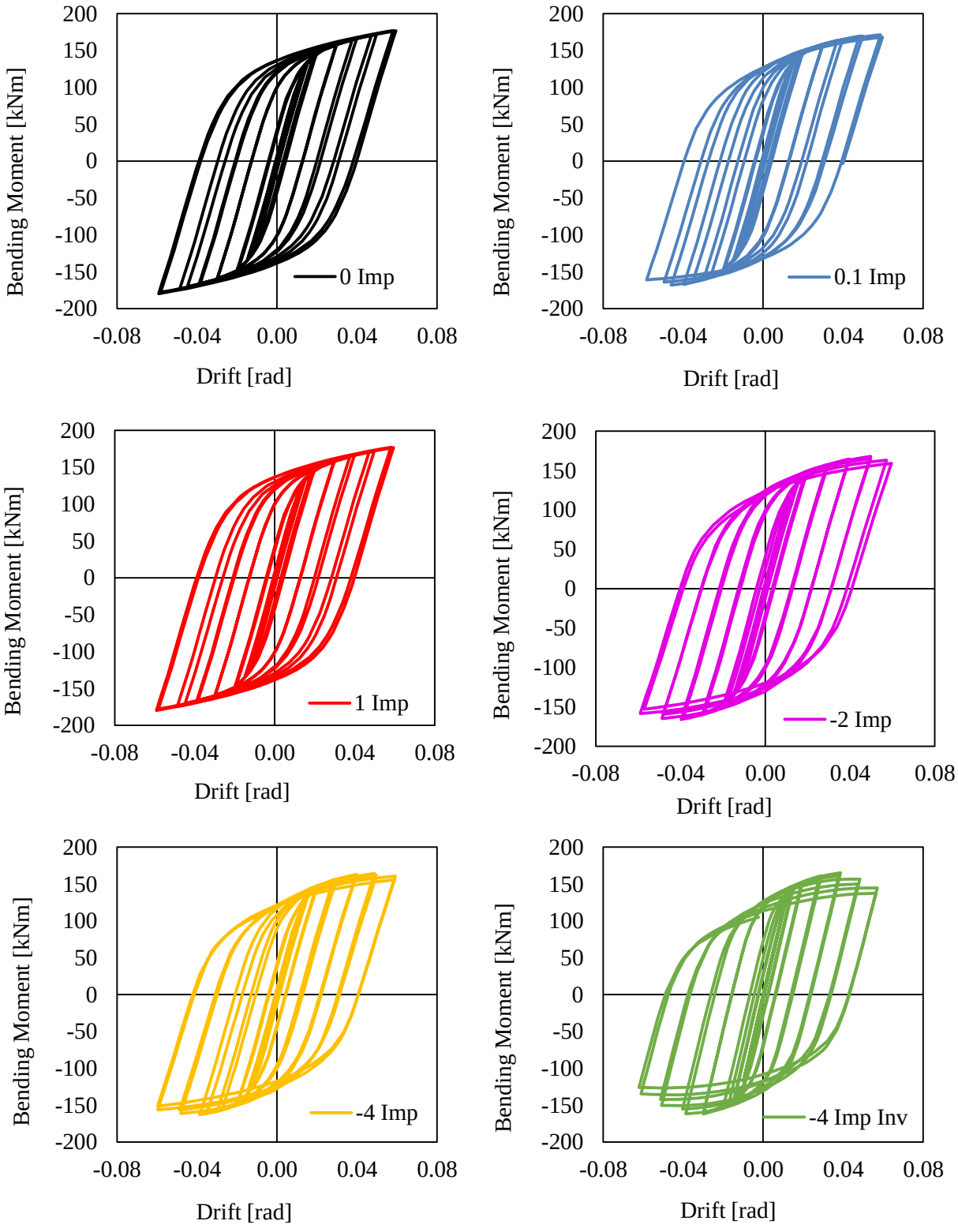

Figure IV.18: Bending moment vs drift

In order to obtain the best numerical results, the bending moment data from numerical analysis should closely resemble that of the experimental results. In order to calibrate our models, previous experimental data was compared to these numerical results.

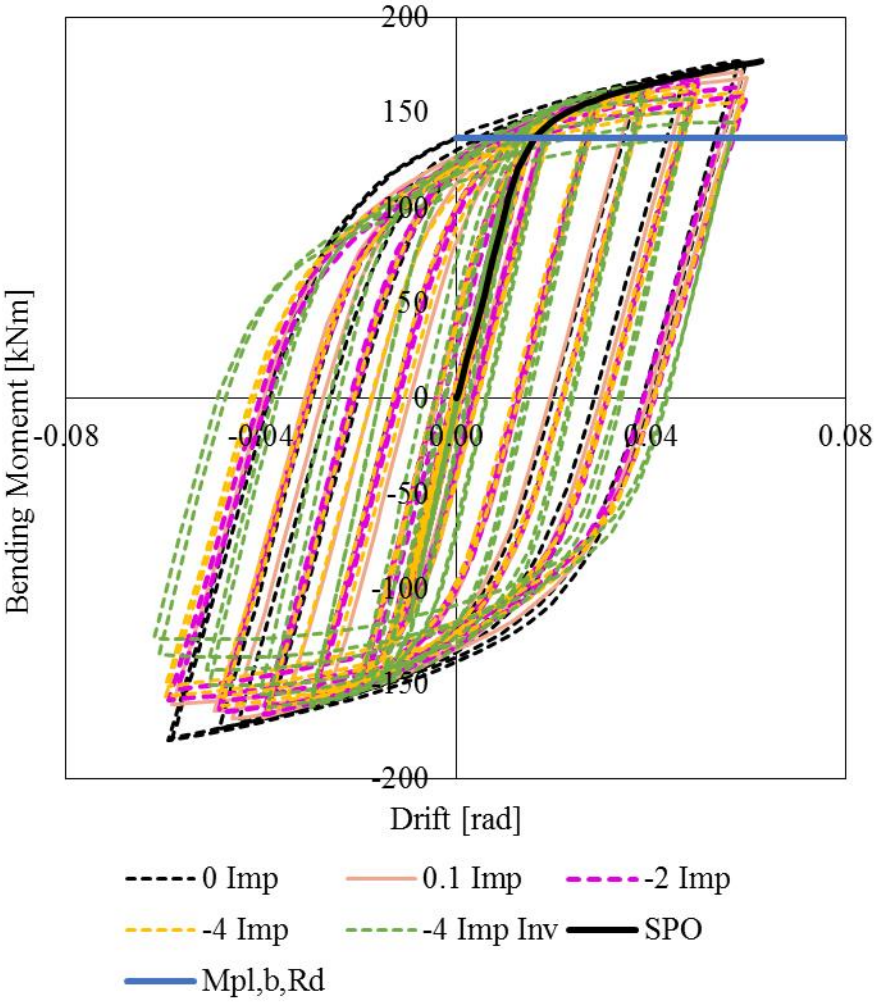

Figure IV.20: Bending moment-drift relation, imperfections test

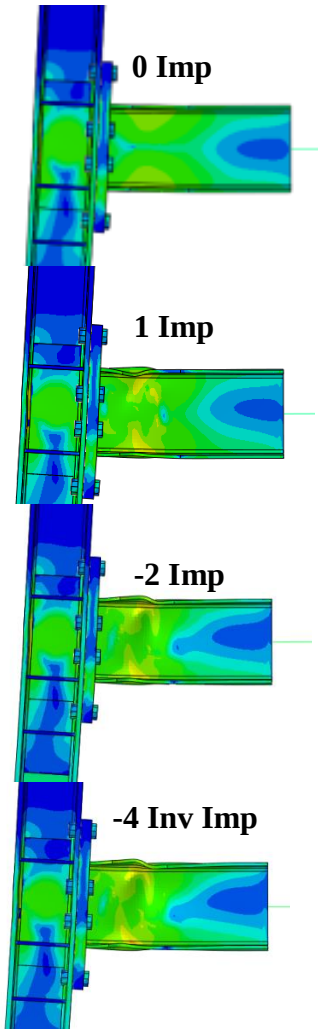

Figure IV.19: Van Mises at joint level

From the previous graphs, it is clear that the model with -4 inversed imperfections is losing the most bending moment capacity with regards to the increase in drift. When comparing this numerical response to the experimental FD hysteric response from **Iannone et al., 2011,** it is clear that the previously mentioned model of imperfections is the one which most closely fits the empirical data. Therefore, this is our best-guess of the realistic imperfections for FD joints. However, more testing would have to be conducted to determine more accurately what is the best fit model.

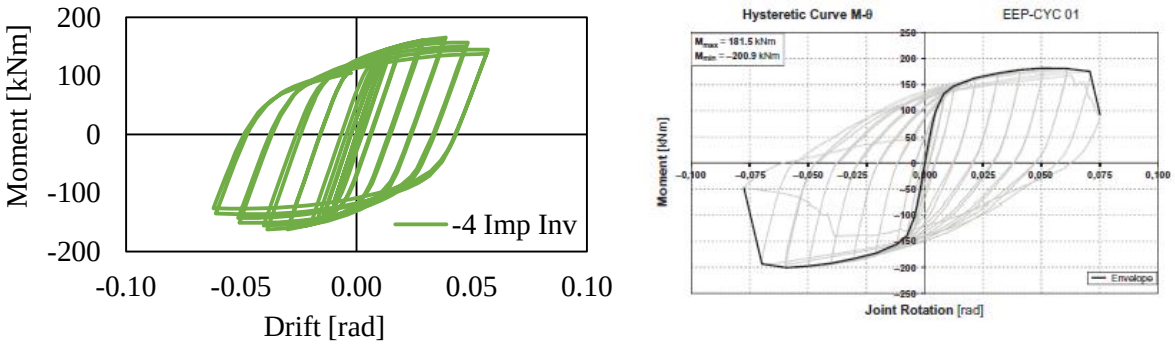

Figure IV.21: Comparison of empirical to numerical data, (Iannone, Latour and Piluso)

4.3.3 Numerical Comparison of FD MRF to RBS MRF

Single story Frames

In the following models, we compare the responses of one-story frames modeled with both RBS joints and FD2 joints. Because of time constraints, the previous parameters were only investigated in this research; they were not implemented into the following models. First we can compare the 1 story models for each joint.

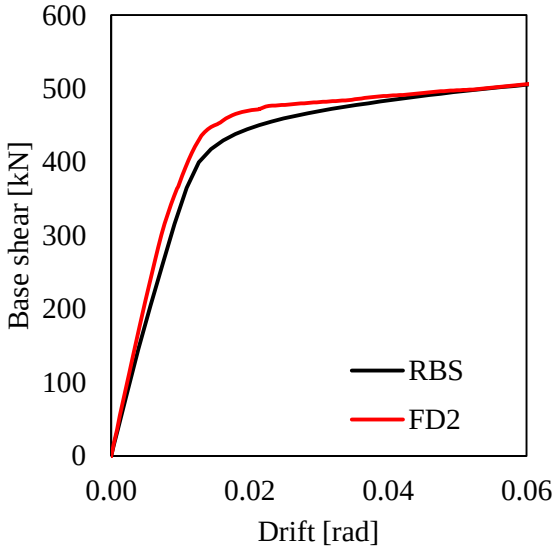

Figure IV.22: Comparison through static nonlinear analysis

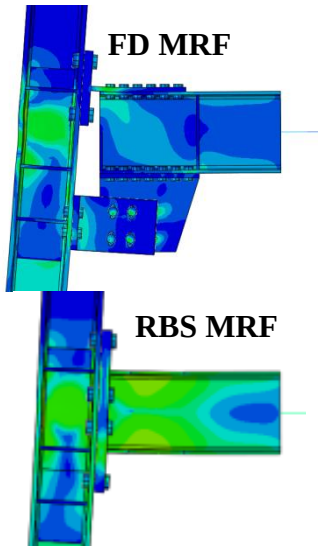

Figure IV.23: Von Mises stresses

From the pushover analysis, we can see that the two frames have a very similar base shear response, with the FD MRF yielding slightly later than the RBS. Even despite this small difference at the point of yielding (or slippage for FD joint), the two frames arrive at exactly the same base shear capacity past 0.05 rads. Another thing to notice is that when FD joints are

implemented in a full frame, the post-slip structural response is much smoother and more linear than the joint level response, which for FD2 joint configurations is mostly saw-toothed in shape. Unfortunately, the cyclic responses cannot be compared so well, as the two time history analyses for the single story FD frame were aborted prematurely, only giving data up to 0.03 rad of drift. From this data we can see that the two responses appear to be similar up to 0.03 radians, however more data is needed. The problem should be corrected and the analyses should be run again with different parameters.

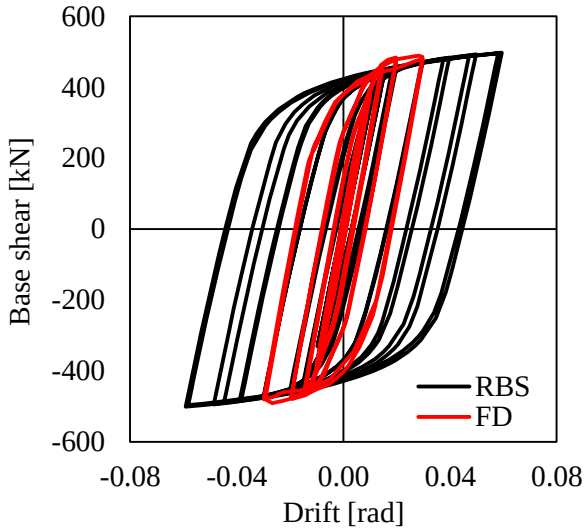

Figure IV.24: MRF responses of RBS and FD frames

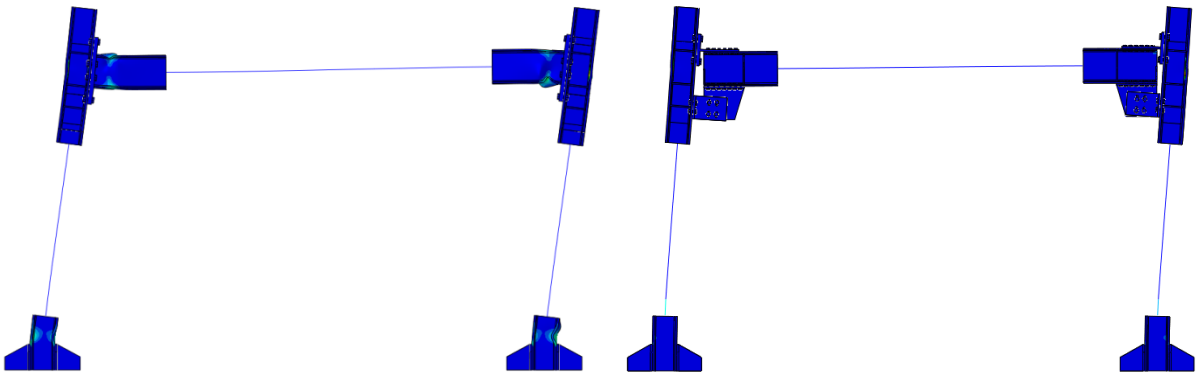

Figure IV.25: Deformed shape of RBS MRF (right) and FD MRF (left)

Two Story Frames

In the following models, we compare the responses of two-story frames modeled with both RBS joints and FD2 joints. First, we will examine the dynamic nonlinear analysis for RBS models.

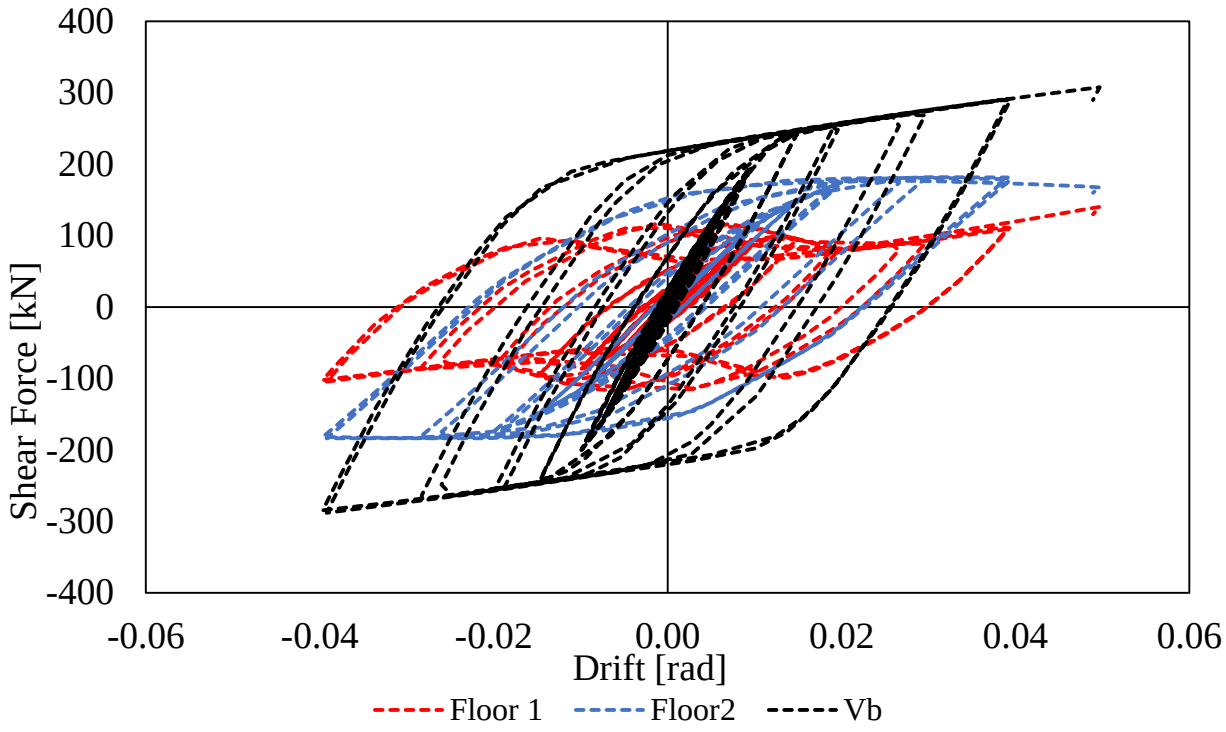

Figure IV.26: Interstory shear forces for 2 story RBS MRF, Imperfections = 1

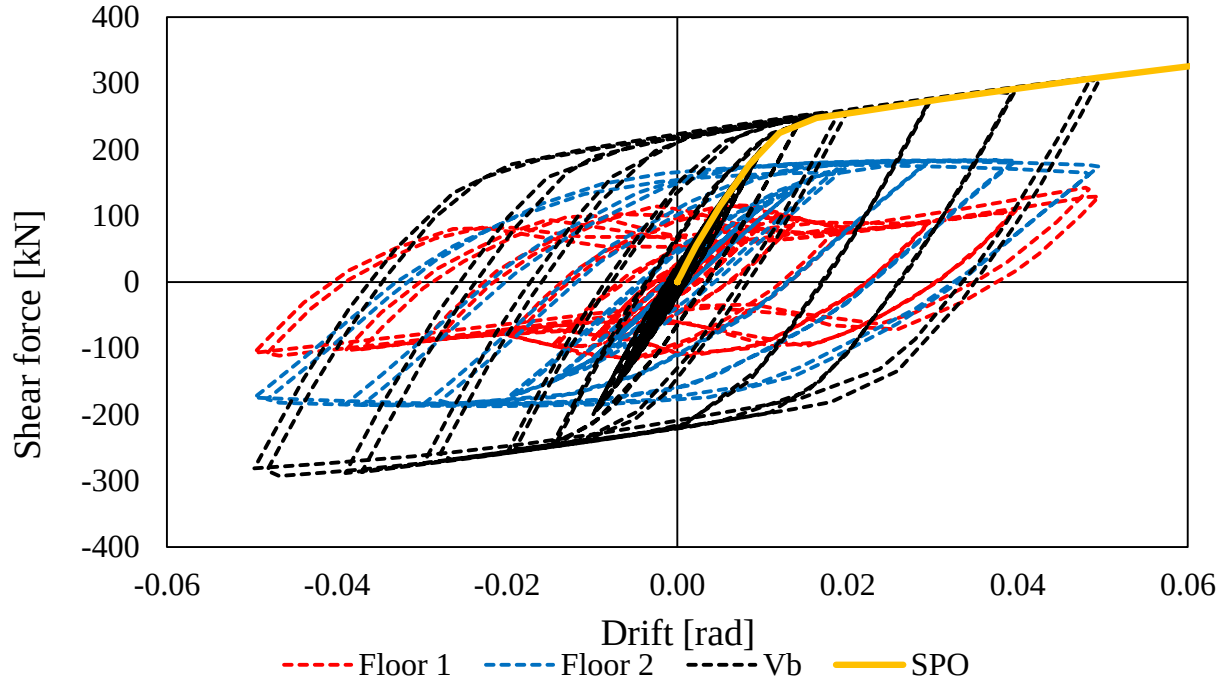

Figure IV.27: Interstory shear forces for 2 story RBS MRF, Imperfections = 4

What is interesting to notice from the previous graphs is that while the base shear and 2nd story shear forces display a regular hysteric loop, the first story shear response is more irregular with respect to drift. This is because of its interaction with the second story. Also, it can be seen that the model with an imperfection of 4mm is slightly more skewed than the previous model with only 1mm of imperfection. Next, we examine the bending moments on each floor of the RBS MRF.

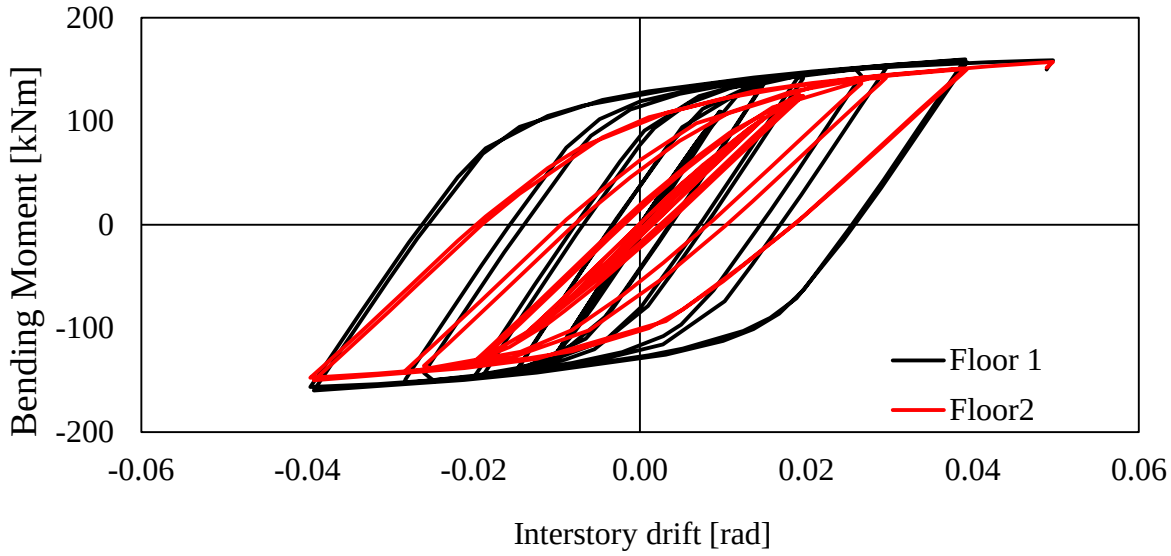

Figure IV.28: Bending moments at floor level, Imperfections =1

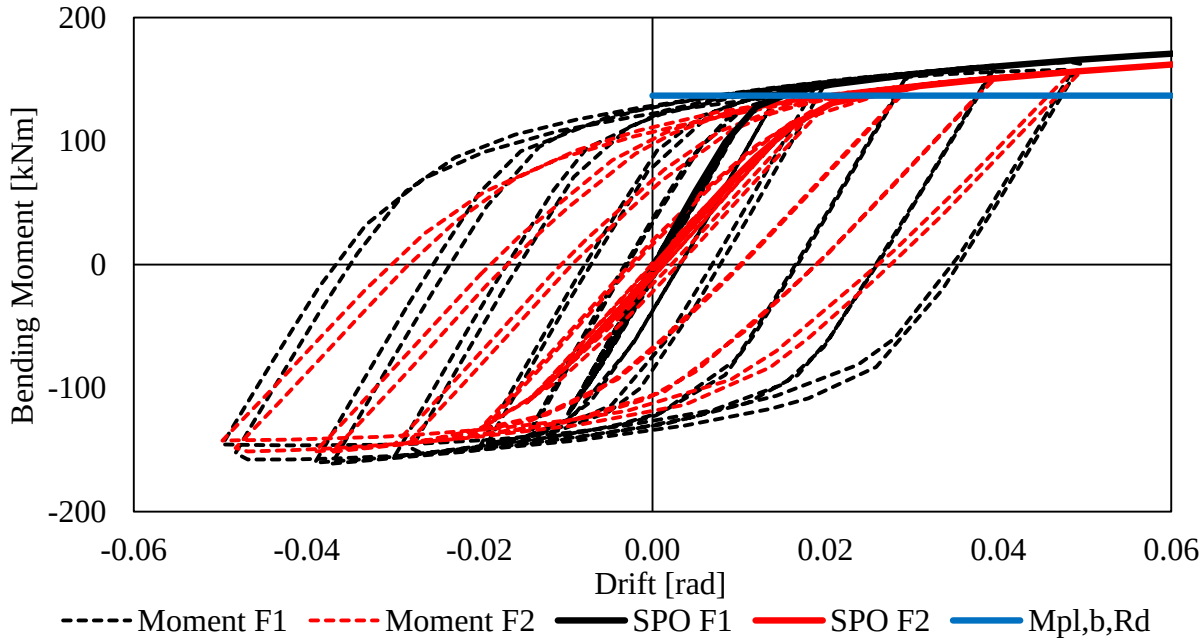

Figure IV.29: Bending moments at floor level, Imperfections = 4

It can be observed that the bending moment capacity of the first floor is higher than the second floor for the same degree of interstory drift. Unfortunately, the time history analysis for FD MRF was again aborted, so we were not able to compare the response of the RBS against FD. However, we are able to compare the static nonlinear responses of both frames.

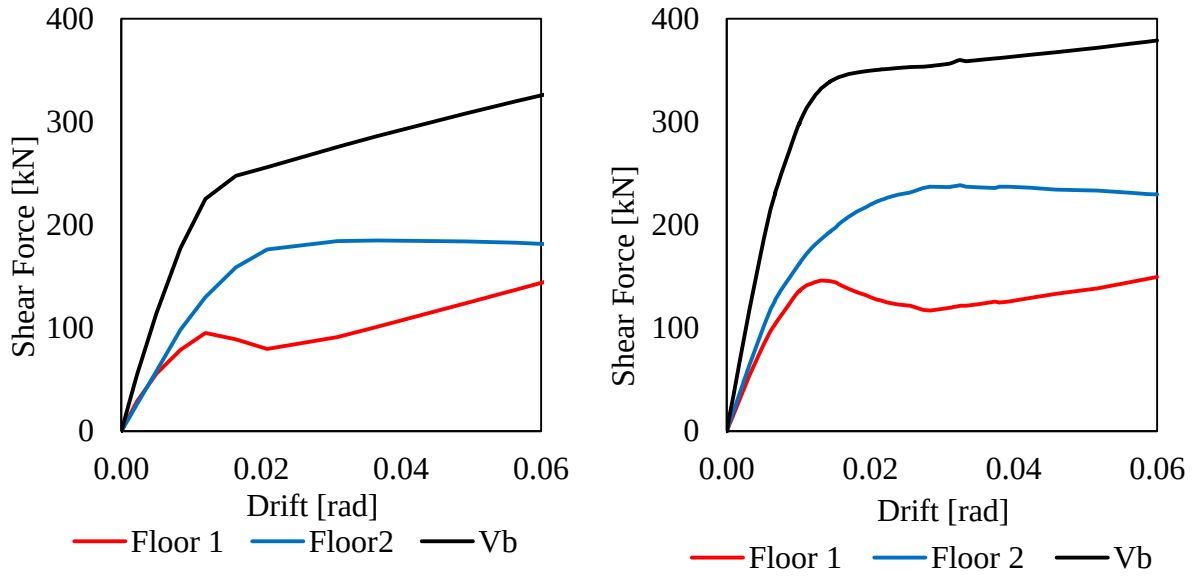

Figure IV.30: Interstory shear force; LEFT- RBS, RIGHT –FD

From the shear force-drift relation, we can observe that the RBS MRF has a much lower capacity than the FD MRF, yielding ~100kN earlier according to the base shear curve. It can also be noticed that the post-yielding behavior of the RBS frame is steadily increasing, while the post-yielding of the FD frame is more static. However, the shear-drift relation at the individual story level appears to be more similar for both frames, although the FD frame's capacity is still higher.

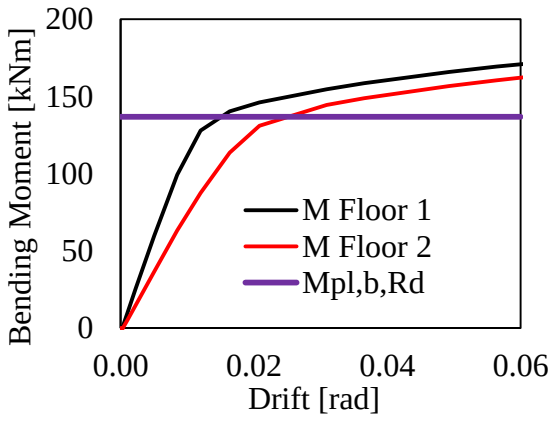

Figure IV.31: Moment-drift relation, RBS MRF

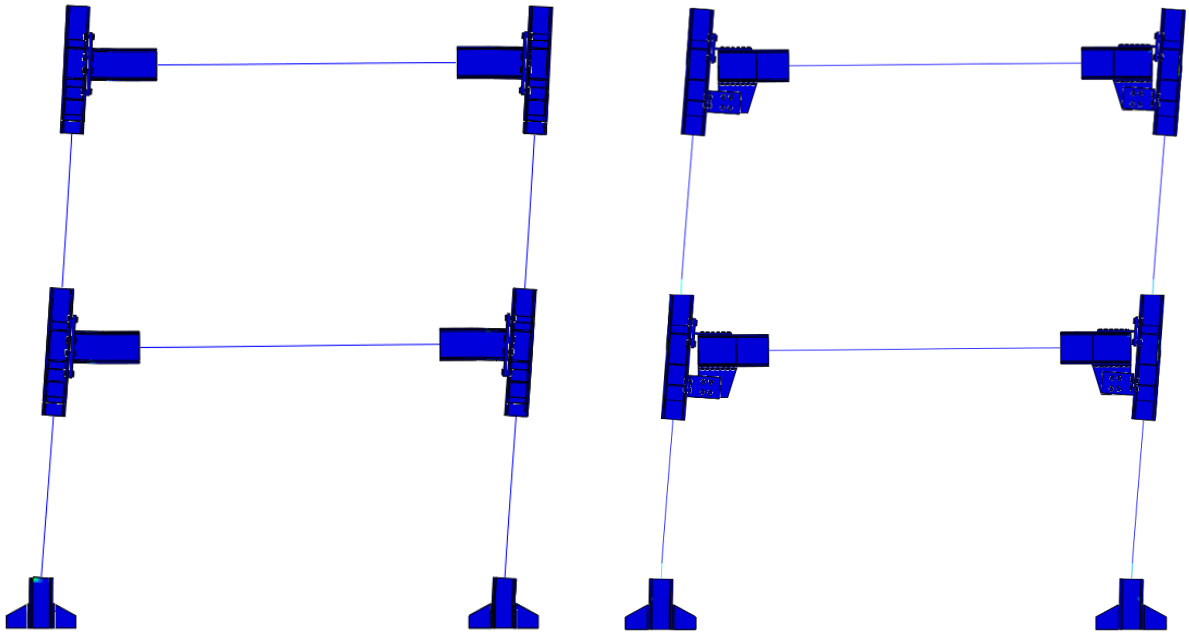

4.4 Investigation into the addition of washerplates into FD joints

During the ongoing tests of FREEDAM joints, a new theory was hypothesized: Would the pre-tensioned bolts in the friction device be more effective if used in conjunction with "washer-plates"?

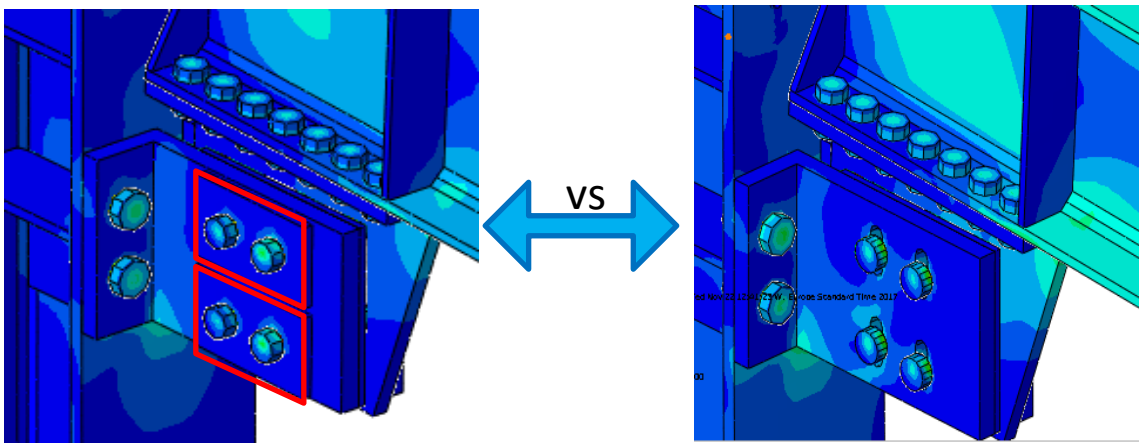

Figure IV.32: Visual comparison of FD joint with and without washerplates

Due to the nature of having slotted holes in the FD connection, the pretensioned bolts heads used to provide a clamping force are not in full contact with the L-stubs. Thus, the application of the

bolt force in the damping device is not fully efficient. By using washer-plates to cover the slotted holes, we would allow the pretensioned bolt heads to remain in full contact with the device. In response, it was expected that the joint will retain more strength and will display a smoother behavior after slippage occurs.

Testing was performed on single joint models.

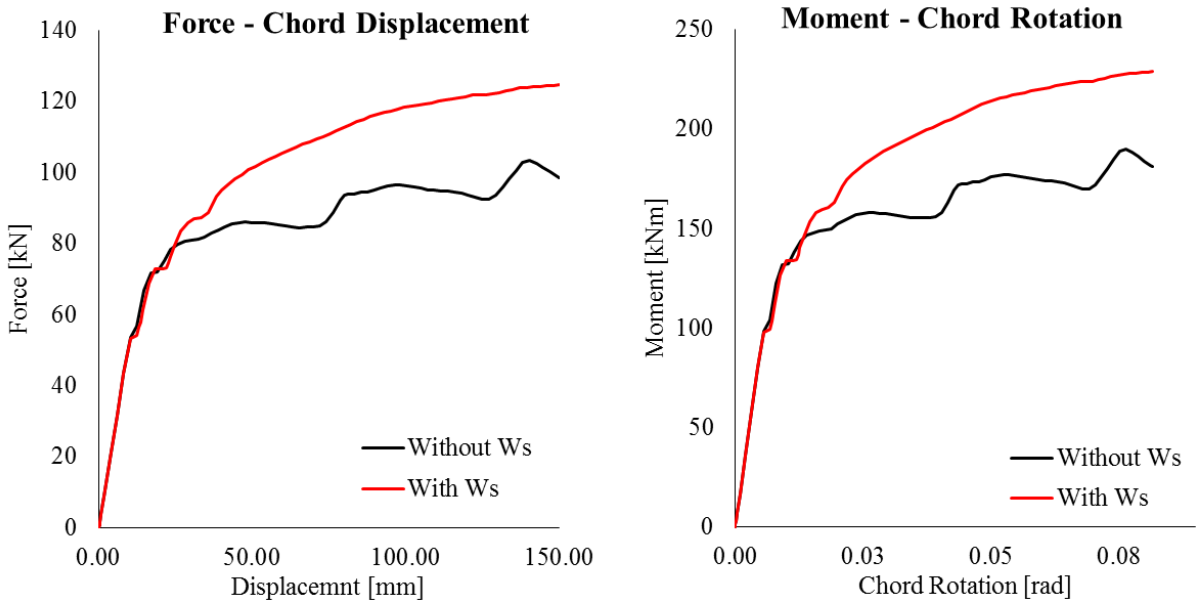

Figure IV.34: Response of joints under negative bending (hogging)

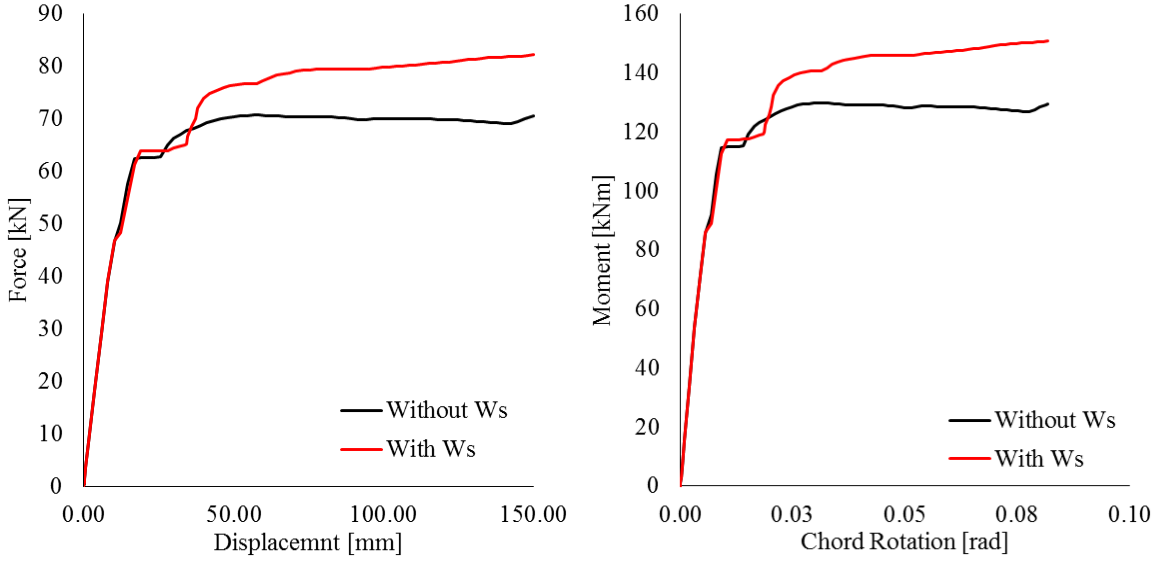

Figure IV.33: Response of joints under positive bending (sagging)

The first step in testing this hypothesis is to compare both joint responses under monotonic loading in a quasi-static nonlinear analysis. In each test, a 150mm displacement was applied to the free end of the beam over a linearly increasing time period, as given by the 'Loading' amplitude in Chapter III. With a chord length of 1865mm, this displacement corresponds to a chord rotation of 8%.

From this response of the joint under hogging moment, it is easy to observe that the washer-plates make a significant difference. Under 0.05rad rotation, there is still up to 29% increase in capacity of the joint. The post-slip response with the new plates is also smoother than the saw-tooth curve the joint without washer-plates.

Similar to before, the joint with washer-plates displays a higher capacity under sagging moment after slipping has occurred, up to 14% increase under 0.05 rad. In this case, both models display planar, nearly horizontal post-slip behavior. While there is evidence from the monotonic nonlinear analysis that washerplates carry a significant benefit to the overall performance of the joint, it is not the full picture. In order to view the full seismic response, a cyclic loading analysis was performed on both joints using a loading amplitude as defined by AISC protocol. Below is the response of both joints.

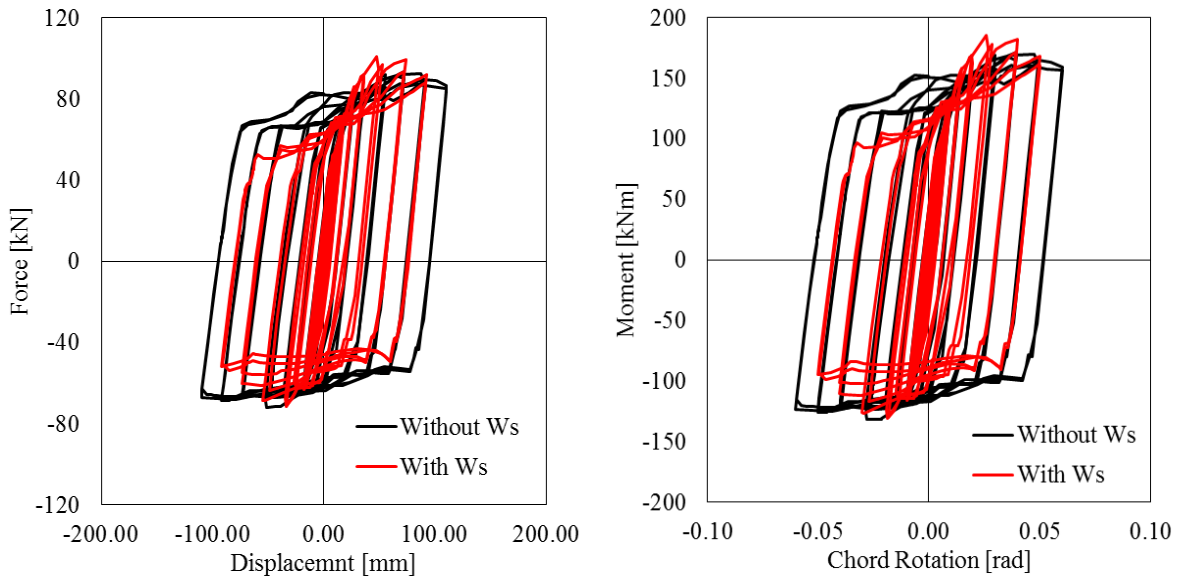

Figure IV.35: Hysteric response of washerplate test

The analysis shows an unexpected response. While the joint with washer-plates shows an initially higher resistance under sagging moment, after repeated cyclic loading the joint loses capacity and becomes weaker than the joint without washerplates.

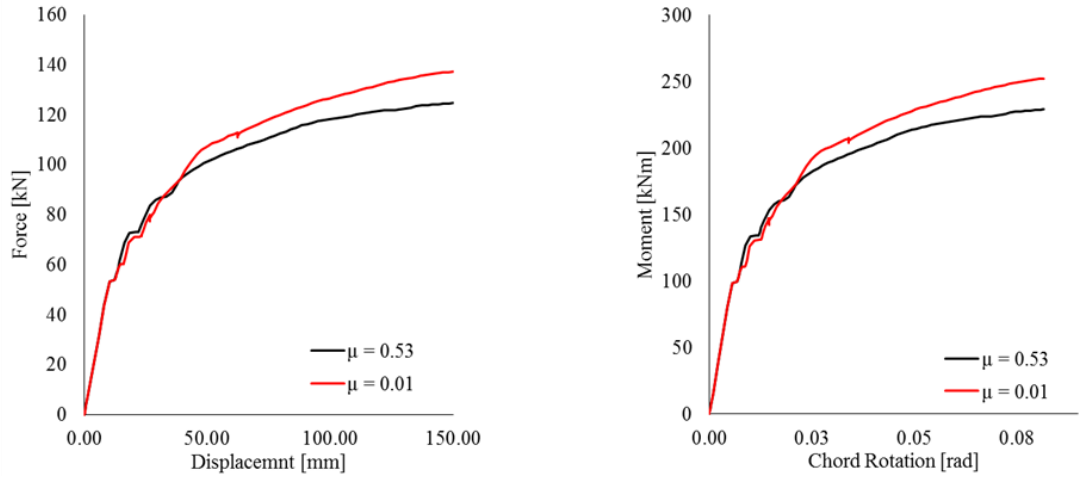

Figure IV.36: Effect of friction on washerplates

Along with this, the additional strength previously seen in the monotonic loading tests, is not able to develop under negative moment. The reasoning for this behavior is unclear; however, there are a few predictions. Because the washerplates are allowed to slide against the L-stubs, it is possible that this interaction was the reason behind the decay of capacity. Thus, the model was re-run with a near-zero friction coefficient on the washerplates (μ=0.01) to see if this was indeed the case.

While there is a slight difference of 7% between the two tests, the extra friction from the washer-plates is not significant enough to be the cause of the strength degradation.

The reason behind this phenomenon has yet to be discovered. One current theory is based on the fact that the already long bolts used in for clamping the friction joint need to be elongated another 20mm to accommodate the washer-plates. This extra length induces some detrimental bending effects within the bolt during sliding, which induces axial eccentricities and decreases the clamping component of the pretension force within the bolts.

While this hypothesis has not be verified, it is corroborated by the ABAQUS model where the clamping bolts do in fact lose pretension force.

After these findings, it was concluded that washerplates should not be used in the friction damping device, as doing so would cause a significant degradation of joint strength under cyclic loading.

4.5 Numerical behavior of selected FREEDAM joint assemblies

Joint Typologies

One main objective of FREEDAM is to develop standardized joint typology which can be used for any size MRF connection. This process involves modelling and analyzing varying sizes and geometries of friction devices and connections to better understand their behavior.

In order to realize the response of different sizes and geometrical configurations of FD joints, three beam-to-column assemblies were selected for the investigation of joints equipped with the designed devices:

- IPE360 / HE 360 B
- IPE550 / HE 500 M
- IPE750x147 / HD 400x634

From these three assemblies, each one was assigned to two different damper geometries, for a total of six different models, as shown in Table IV.3 and Figure IV.37.

Table IV.3: Details of FD assemblies

ID	Beam	Column	L	H	Bolts	No. Bolts	n_b			
			mm	*mm*			0.3	0.4	0.5	0.6
D1	IPE360	HE 360B	3000	3500	M16	4	0.42	0.55		
D2-A	IPE360	HE 360B	3000	3500	M20	4			0.41	0.49
D2-B	IPE550	HE 500M	3000	3500	M20	6		0.45	0.57	
D2-C-I	IPE550	HE 500M	3000	3500	M20	8			0.43	0.51
D2-C-II	IPE750X147	HD 400X634	4000	4000	M20	8		0.5	0.62	
D3	IPE750X147	HD 400X634	4000	4000	M24	8			0.39	0.47

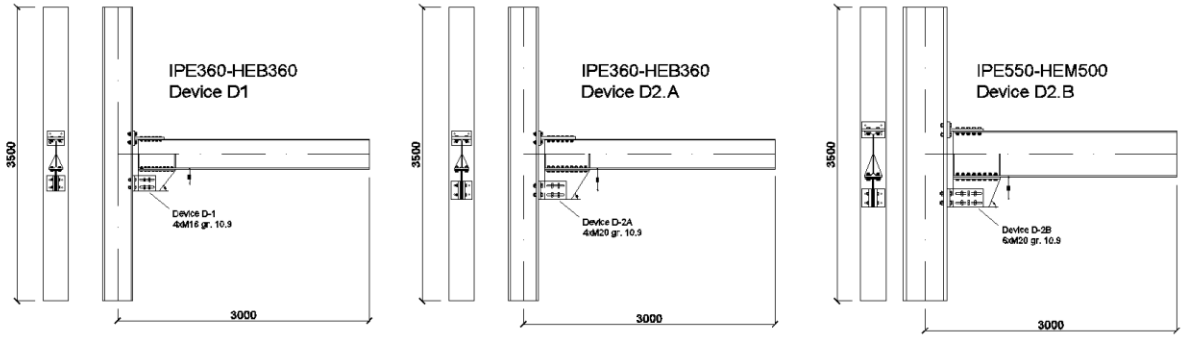

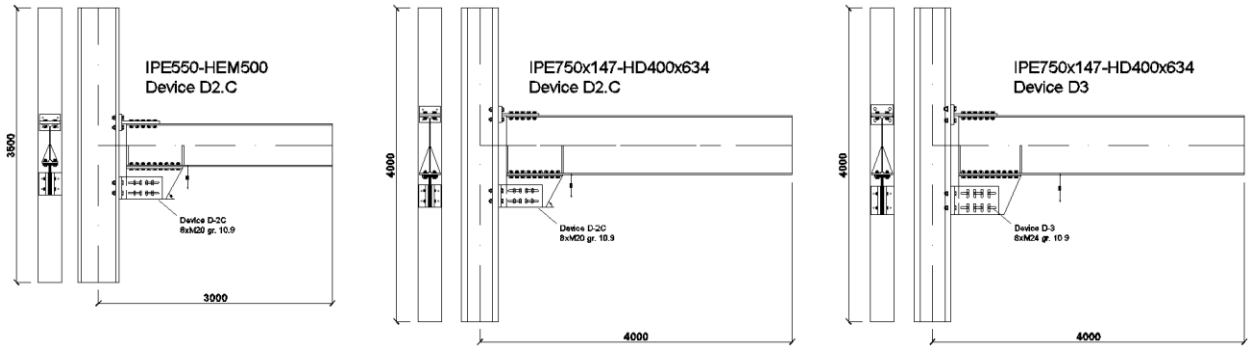

Figure IV.37: Modeled FD joint geometries

Before the joints were modeled, it was determined whether or not additional web panels were needed to supplement the shear panel of the column. The calculations were conducted according to EN 1993-1-1 using the following formula for web panel shear verification:

$$V_{wp,Rd} = \frac{0{,}9 f_{y,wc} A_{vc}}{\sqrt{3}\gamma_{M0}}$$

Where $V_{wp,Rd}$, is the design resistance of the shear web panel, $f_{y,wc}$ is the yield strength of the column material, γ_{M0} is the material safety factor, and A_{vc} is the shear area of the column as given by EN 1993-1-1:

$$A_{vc} = A - 2bt_f + (t_w + 2r)t_f$$

Where all of the variables in the equation are dimensions of the column section. The column web panel was checked against the joint bending resistance, which was taken as 60% of the beam bending capacity.

$$V_{wp,Rd} \geq \frac{M_{j,Rd}}{z^*}$$

Where $M_{j,Rd}$ is the design joint bending moment capacity and z* is the height of the column shear panel. The joint bending capacity is derived from the beam capacity, as shown below:

$$M_{j,Rd} = 0{,}6 \cdot \Omega \cdot M_{pl,b,Rd}$$

Where Ω is the overstrength factor for the FD joint, which has experimental values ~1.7 but in these calculations it was taken as 2.0 to be conservative.

Table IV.4: Column web panel check

ID	Assembly	$M_{pl,b,Rd}$	$0,6\Omega M_{pl,b,Rd}$	z*	Av	$V_{wp,Rd}$	$M_{j,Rd}/z^*$	Check
		kNm	kNm	mm	mm^2	kN	kN	
D1	IPE360 / HE360B	362	434	540	6113	1128	804	PASS
D2.A	IPE360 / HE360B	362	434	623	6113	1128	697	PASS
D2.B	IPE550 / HE500M	989	1187	813	13687	2525	1461	PASS
D2.C	IPE550 / HE500M	989	1187	844	13687	2525	1406	PASS
D2.C	IPE750x147 / HD400x634	1814	2177	1037	18446	3403	2099	PASS
D2.D	IPE750x147 / HD400x634	1814	2177	1098	18446	3403	1983	PASS

In the end, none of the columns required web panels; however continuity plates were added to keep the column flanges from buckling. Three continuity plates were used on each side of the column. Plates were placed at the same heights as the centers of the T-stub and L-stub, as well as the beam bottom flange. D2.D was run as a static nonlinear analysis.

FD Joint Responses

Because of the time constraints and the length of time it takes to analyze one joint, the models were only able to be run once. For a yet unknown reason, all of the time history analyses aborted between 0.01 – 0.03 radians of rotation. It is estimated that this is the same problem we had with the FD full frame analyses. Although we do not have the full data, there is a lot that can be determined from these graphs. First of all, we can take a preliminary look at the variations between hogging and sagging moments for these six analyses.

Table IV.5: Variation between hogging and sagging moments

ID	m	Variation
D1	0.3	1.19
D1	0.4	1.47
D2.A	0.5	1.22
D2.A	0.6	1.31
D2.B	0.5	1.25
D2.B	0.6	1.35

As can be viewed from Table IV.5, there is significant difference between the moment capacities obtained in hogging and sagging. With variations as high as 47% in the second analysis, the joints can be labeled as highly asymmetric. This is different from previous studies by D'Aniello et al., 2017 regarding FD2 joints, which realized only 14% variation between positive and negative bending moment. This variation was the same regardless of joint size. While this difference may be attributed to the same problem that caused the analyses to abort, it should be investigated further.

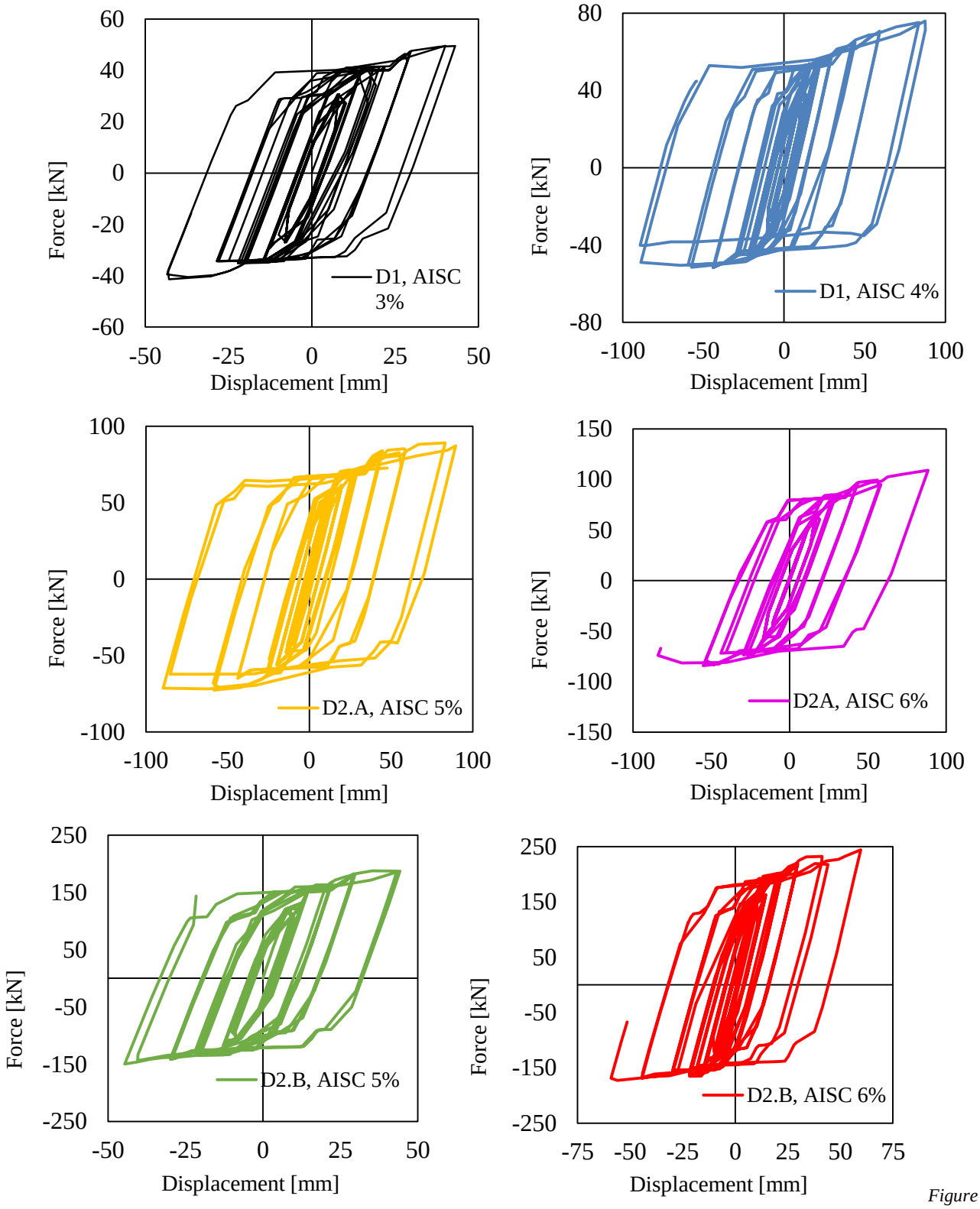

Figure IV.38: Force-displacement relation, FD joints

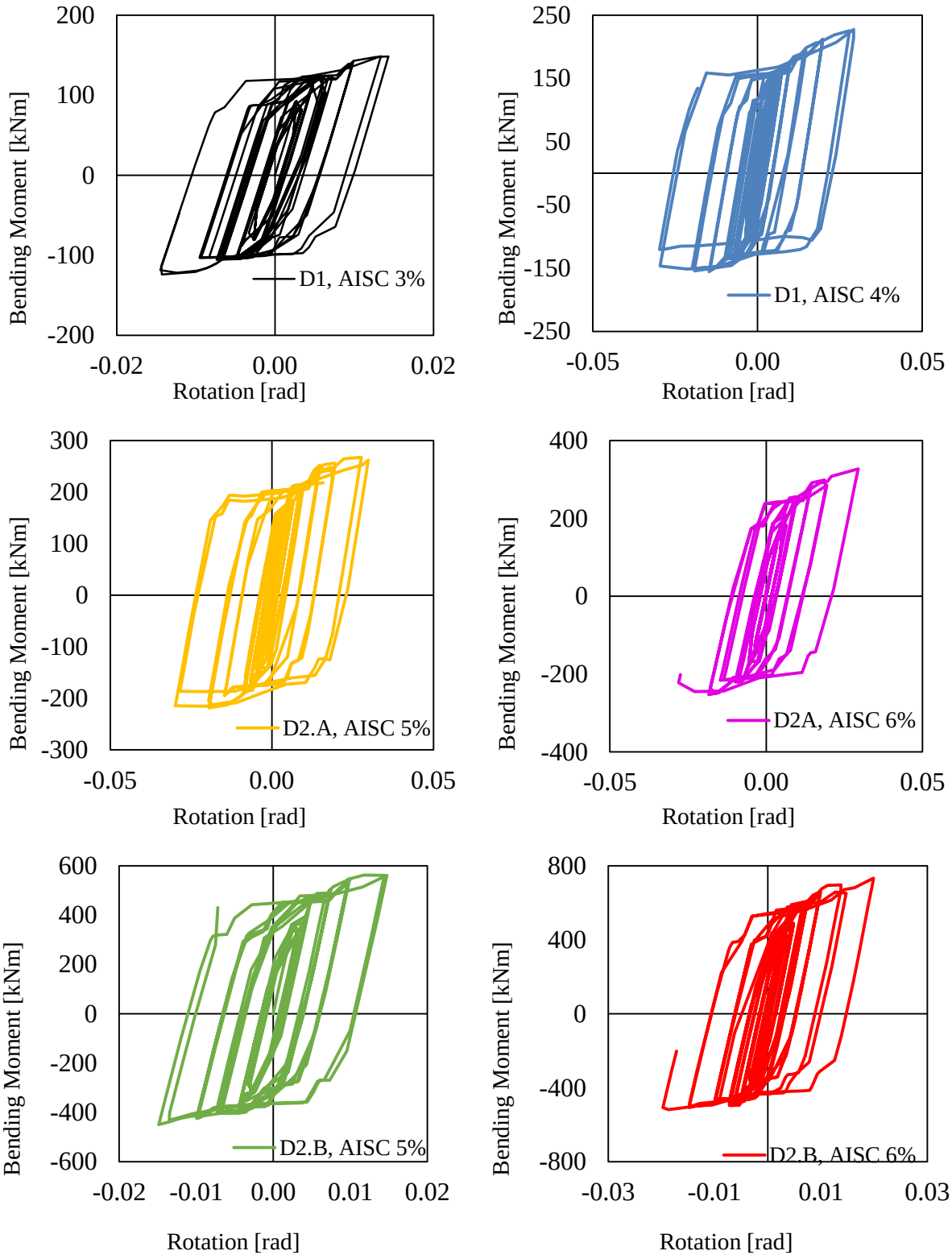

Figure IV.39: Moment-chord rotation graphs, FD joints

While the dynamic nonlinear analyses were not able to be completed, we tested one joint with a static nonlinear and were able to obtain accurate results up to 0.035 radians of rotation. Although this value does not approach the desired 0.05rads, it still gives us a clear image of the post-slip response. The following graphs are from the last and largest joint in the series, FD2.D.

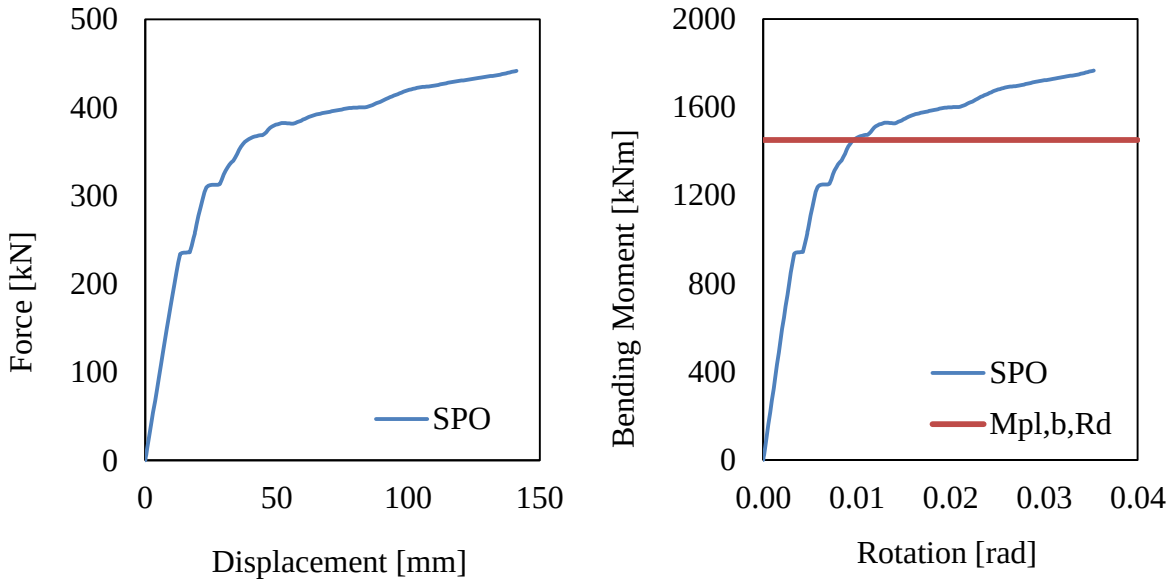

Figure IV.40: Full chord response of joint

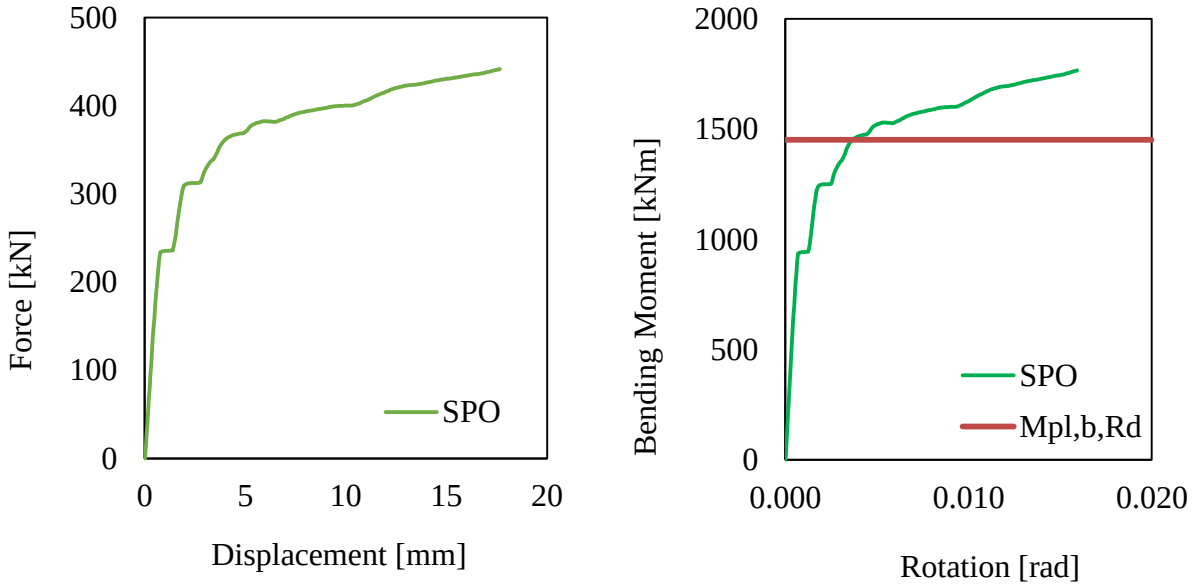

Figure IV.41: Damper response

Chapter V: CONCLUSIONS

From the analyses performed in the previous chapters, the following conclusions can be summed up:

- At a significant distance away from the joint face, wire elements can be utilized to decrease the number of finite elements in the model without having a significant impact on the response.

- Using washerplates would cause a substantial loss of bending moment capacity in FD joints; therefore they should not be used.

- Both static nonlinear and dynamic nonlinear analysis determined that there is no impact on frame response from implementing ductile damage after yielding occurs. What this most likely signifies is that the damage model we used was not a good fit, and therefore should be revised.

- From a comparison of the different time history analyses of the full frames, we were able to determine that imperfections reduce the bending moment and base shear capacity of the model. The imperfection modelling of from the buckling modes with coefficients of -4 inverse was the best fit for the frames, however it was not perfect. This should also be revised. Our material damage model was also incorrect.

- The FD MRF has a slightly higher bending moment capacity than RBF in a one story frame analysis, and significantly higher capacity in two story frame.

- The FD joints show significant promise and the response in positive and negative bending moments are more or less symmetric. However, due to many of the analyses being aborted prematurely for the FD frames, the cause should be investigated and the analyses re-run.

Chapter VI: REFERENCES

[i]ANSI/AISC 341-16. "Seismic Provisions for Structural Steel Buildings." 2016.

Arcelor Mittal. *Section Program*. 2016. <http://sections.arcelormittal.com/fileadmin/redaction/4-Library/1-Sales_programme_Brochures/Sales_programme/Sections_MB-ArcelorMittal_ES_EN_IT-V2016-2.pdf>.

Borzouie, J, et al. "Experimental studies on cyclic performance of column base weak axis aligned asymmetric friction connection." *Journal of Constructional Steel Research 112* (2015): 252-262.

Borzouie, J., et al. "Experiemental studies on cyclic performance of column base strong axis-aligned asymmetric friction connections." *Journal of Structural Engineering* (2016).

Clifton, C, et al. "Sliding Hinge Joints and Subassemblies for Steel Moment Frames." *NZSEE Conference*. 2007. 1-7.

Clifton, C. *Semi-rigid joints for moment-resisting steel framed seismic-resisting systems*. Auckland, New Zealand: Department of Civil and Environmental Engineering, University of Auckland, 2005.

D'Aniello, Mario et al. "Finite element analysis on free from damage seismic resisting beam-to-column joints." *ECCOMAS Thematic Conference on Computational Methods in Structural Dynamics and Earthquake Engineering*. Rhodes Island, Greece, 2017. 1-13.

D'Aniello, Mario, et al. "Development and validation of design criteria for free from damage steel joints." *Eurosteel*. Copenhagen: Ernst & Sohn, 2017.

Dhondt, Guido. *CalculiX CrunchiX User's Manual*. 03 03 2014. http://web.mit.edu/calculix_v2.7/CalculiX/ccx_2.7/doc/ccx/node28.html. 14 11 2017.

Ghosh, Amab and Farshid Sadeghi. "A novel approach to model effects of surface roughness parameters on wear." *Wear* (2015): 73-94.

Iannone, F., et al. "Experimental Analysis of Bolted Steel Beam-to-Column Connections: Component Identificaiton." *Journal of Earthquake Engineering, 15* (2011): 214-244.

Khoo, H.H., et al. "Developments on the Sliding Hinge Joint." *WCEE*. Lisbon, 2012. 1-10.

Khoo, Han-Hsen, et al. "Behaviour of the bottom and top flange plates in the sliding hinge joint." *Bulletin of the New Zealand Society for Earthquake Engineering, Vol. 46, No.1* (2013): 1-10.

Khoo, Hsen-Han, et al. "Development of the self-centering Sliding Hinge Joint with friction rings." *Journal of Constructional Steel Research* (2012): 201-211.

Khoo, Hsen-han, et al. "Proposed design models for the asymmetric friction connection." *International Association for Earthquake Engineering* (2014).

Swanson, J. and R.T. Leon. "Stiffness modeling of bolted T-stub connection components." *Journal of Structural Engineering* (2001): 498-505.

United States Geological Survey. *Earthquake Facts and Statistics*. 29 November 2012. <https://earthquake.usgs.gov/earthquakes/browse/>.

Zimbru, Mariana, et al. "Performance assessment and design methodology of free from damage moment resisting frames." *Eurosteel*. Copenhagen, Denmark: Ernst & Sohn, 2017. 560-569.